UNIVERSITY OF SPLIT

SCHOOL OF MEDICINE

mr. sc. Viktorija Radotić, mag, struc. and funct. biol.

MORPHOLOGICAL AND ELECTROPHYSIOLOGICAL CHARACTERIZATION OF SPIRAL GANGLION NEURONS *IN VITRO* CULTURED ON HIGH-DENSITY COMPLEMENTARY SEMICONDUCTOR ELECTRODE ARRAY

Doctoral dissertation

Academic year: 2023/2024

Mentor:

Associate Professor Damir Kovačić, PhD

In Split, 2024

Mentor: Associate Professor Damir Kovačić, PhD

THANKS

I thank my mentor, Damir Kovačić, for mentorship and all support. I also thank all my colleagues from the laboratory for assistance and advice during my laboratory work: Professor Damir Sapunar for technical support and advice, Professor Ante Bilušić from the Faculty of Science, and Jasna Arapov and her co-workers from the Institute of Oceanography and Fisheries (Split) for the SEM microscopy assistance, Jordi Cools from imec vzw (Leuven, Belgium) for the SEM protocol, Jagoda Dujić from the University of Split for help from the animal facility and Dries Braeken and Beatrice Miccoli from imec vzw (Leuven, Belgium) for helping me to conduct the electrophysiological experiments.

CONTENT

TABLE OF FIGURES

Abbreviations

BDNF	Brain-derived neurotrophic factor
BSA	Bovine serum albumin
CI	Cochlear implant
CMOS	Complementary metal-oxide-semiconductor
DAPI	4,6-diamidino-2-phenylindole
DCN	Dorsal cochlear nuclei
DIV	Days *in vitro*
DMEM	Dulbecco's modified eagle medium
EAP	Extracellular action potential
FBS	Fetal bovine serum
FFT	Fast Fourier transform
GDNF	Glial cell line-derived neurotrophic factor
HCs	Hair cells
HPW	Highly purified water
IHCs	Inner hair cells
MEA	Microelectrode array
MPS	Micro pillar substrates
NT-3	Neurotrophin 3
OHCs	Outer hair cells
PBS	Phosphate buffered saline
PCB	Printed circuit board
PDLO	Poly-DL-ornithine

RA	Rapid accommodating
ROI	Region of interest
SA	Slowly accommodating
SD	Standard deviation
SEM	Scanning electron microscope
SGNs	Spiral ganglion neurons
SNHL	Sensorineural hearing loss
VCN	Ventral cochlear nuclei

DISCLOSURE

This thesis has incorporated data and figures from the following publications I co-authored and which were published during my doctoral study:

Radotić V, Braeken D, Drviš P, Mattotti M, Kovačić D. Advantageous environment of micro-patterned, high-density complementary metal-oxide-semiconductor electrode array for spiral ganglion neurons cultured *in vitro*. *Sci Rep.* 2018, 8: 7446.

Radotić V, Braeken D, Kovačić D. Microelectrode array-induced neuronal alignment directs neurite outgrowth: analysis using a fast Fourier transform (FFT). *Eur Biophys J*. 2017, 46: 719-727.

Radotić V, Bedalov A, Drviš P, Braeken D, Kovačić D. Guided growth with aligned neurites in adult spiral ganglion neurons cultured *in vitro* on silicon micro-pillar substrates. *J Neural Eng*. 2019, 16: 066037.

1. INTRODUCTION

The auditory system significantly impacts communication in humans [1]; therefore, hearing loss, a disease with an increasing incidence in industrial countries, is an insidious issue that decreases quality of life [1, 2]. Hearing impairment usually stems from the loss of inner and outer hair cells (HCs), the sensory cells of the inner ear [3], which is often followed by degeneration of primary cochlear afferent neurons, the spiral ganglion neurons (SGNs) [3]. SGNs are critical for hearing as they transmit auditory information through electrical signals from the inner ear's mechanosensory hair cells to the brain stem's cochlear nuclei [1]. Besides transmitting frequency information, SGNs must preserve sound stimuli's fine structure, code signals with sub-millisecond precision, and transmit signals of various intensities sustainably [4]. The progressive degeneration of these auditory neurons and the loss of inner hair cells cause sensorineural hearing loss (SNHL), affecting hundreds of millions worldwide [1, 2]. This can be due to many causes, including aging, noise exposure, and ototoxic drugs [5, 3]. In cases of profound and severe SNHL, resulting in deafness, central auditory function, like hearing, can be restored via electrical stimulation of surviving SGNs with a cochlear implant (CI) in humans [3]. As SGNs can also degenerate as a result of noise exposure and aging, while HCs remain intact, they are a primary target for regeneration, and a better understanding of morphological and electrophysiological aspects of these neurons may ultimately result in long-term maintenance of hearing loss and accelerate regenerative therapies [1, 3].

Cochlear implant (CI) is currently the prevailing neuro-prosthetic treatment for partial restoration of hearing in deaf people. It comprises a linear electrode array, containing up to 26 electrodes, that is surgically inserted into the cochlea, typically within the perilymph-filled scala tympani [6]. This arrangement functionally bypasses some or all of the approximately 3,400 malfunctioned hair cells by directly stimulating preserved spiral ganglion neurons, which form the auditory nerve [7, 8]. Due to the limited spectro-temporal information delivered with electrical stimulation, speech perception as well as listening to music are still rather inadequate in the majority of CI users, especially in real-world settings [9]. The neuron-electrode interface plays a crucial role in the neural coding of auditory information. Our approach to overcome the major constraint of non-focal and non-selective electrical stimulation of SGNs in current CI devices is based on the substantial increase in the number of stimulating electrodes and the significant reduction in the size of stimulating electrodes, similar to cellular dimensions of SGNs. This approach targets decreased not only SGN survival, which largely depends on the duration and etiology of deafness

but also the anatomical gap between the implanted electrode array and the stimulated regions of the auditory nerve [7, 8, 9, 10, 11, 12, 13].

1.1 Auditory system

The auditory system is comprised of four main sections: the outer ear, middle ear, inner ear, and brain. The outer ear is comprised of the pinna (or visible ear) and ear canal, constructed from elastic cartilage, and ends in the eardrum [14]. The shape of the pinna aids our ability to locate sounds, while the canal's dimensions amplify the weaker and higher-pitched consonant frequencies in speech [14]. The middle ear, beginning at the eardrum and ending at the cochlea, comprises the three smallest bones: malleus, incus, and stapes [14]. Here, the sound waves are changed from the acoustic energy captured by the outer ear to mechanical energy; the mild leverage action of these bones amplifies this energy [14]. The inner ear comprises the coiled cochlea, which is connected to the three semicircular canals by the vestibule, providing a sense of balance [14]. This snail-shaped organ changes the incoming mechanical energy to hydraulic energy as it flows through this fluid-filled organ [14]. There, water-like ripples undulate a membrane lined with 20-30,000 tone-specific receptor cells and, in turn, create nerve impulses which are then fed to the brain via the acoustic nerve [14]. The cochlea makes 2-1/2 turns in the human and consists of three channels divided by two thin membranes. The top tube is the *scala vestibuli*, connected to the oval window [14]. The bottom tube is *scala tympani*, which is connected to the round window. Both scalaes are located within the bony labyrinth, which is filled with perilymph (poor in potassium ions), a fluid similar in composition to cerebrospinal fluid [14]. The middle tube is the scala media, filled with endolymph (rich in potassium ions), a fluid similar in composition to the intracellular fluid found inside cells [14]. Scala media contains the Organ of Corti [14]. The Organ of Corti sits one the basilar membrane, which forms the division between the scala media and scala tympani and is composed of mechanosensory cells, known as hair cells [14]. There are three rows of outer hair cells (OHCs) and one row of inner hair cells (IHCs). 95% of the VIIIth nerve afferents synapse on inner hair cells, and about 5% of the afferents synapse with outer hair cells [14]. Tiny finger-like projections known as stereocilia are found on top of the hair cells, and they are organized in the gradual manner with the shortest cilia on the outer rows and the longest ones in the center [14].This arrangement allows the sensory cells superior tuning capability [14]. Stereocilia of the hair cells are surrounded by endolymph, rich in potassium ions, and when the sound waves move the hair cells, stereocilia cation channels are pulled open, and potassium, as well as calcium ions, flow into the top of the hair cell. With this influx of positive ions, the IHCs become depolarized, opening voltage-gated calcium

channels at the basolateral region of the hair cells an triggering the release of the neurotransmitter glutamate. An electrical signal is then sent through the auditory nerve and into the brain's auditory cortex as a neural message [14].
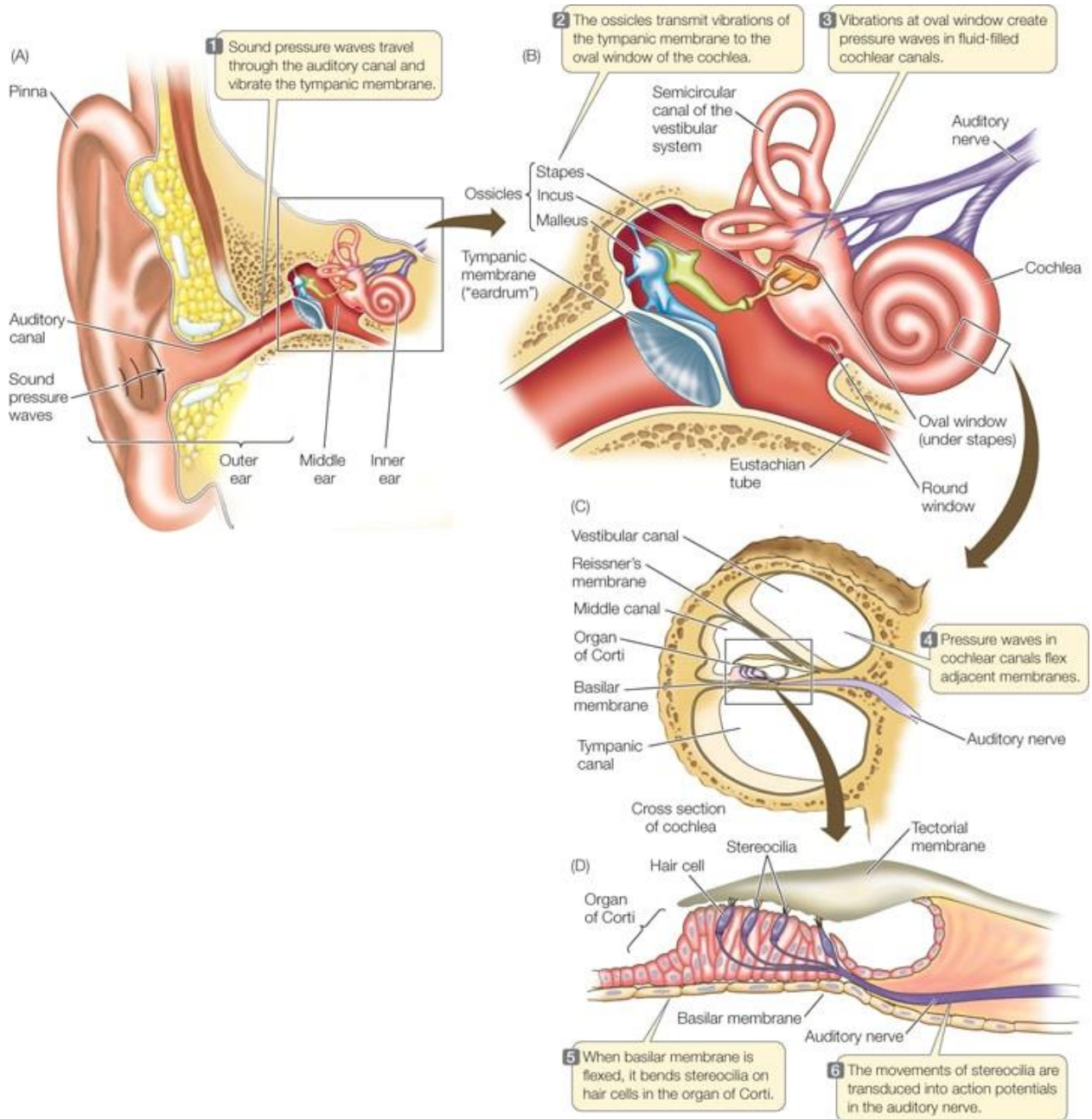
Figure 1. Auditory system (downloaded from www.macmillanhighered.com). Sound waves are collected by the outer ear and are funneled through the ear canal to the eardrum. Sound waves cause the eardrum to vibrate. The three bones of the middle ear (malleus, incus, stapes) transmit and amplify the vibrations to the oval window of the inner ear. Fluid in the inner ear stimulates nerve endings called hair cells. Electrical impulses are sent from the hair cells along the auditory nerve to the brain.

1.2 Spiral ganglion neurons (SGNs)

The mammalian cochlea, in the shape of a coil, contains cells of different types to efficiently relay sound from our surroundings to the brain [15]. Mechano-sensitive hair cells (HCs) and the spiral ganglion neurons (SGN), are two major sensory cell types with the dominant roles in the auditory system. SGNs are bipolar neurons that extend their peripheral axons (sometimes called "dendrites") to HCs and central processes that typically branch into individual processes going towards dorsal (DCN) and ventral (VCN) cochlear nuclei in the brainstem [15, 16]. Two types of neurons have been identified in the spiral ganglion [15, 16]. Type I neurons are large and bipolar cells representing 90-95% of the total number of SGNs, and their peripheral processes innervate single inner hair cells [IHCs, 15, 16]. Cell bodies of Type I SGNs and their processes are covered with myelin sheaths, except in humans, where the lack of somatic myelination can be observed [17]. Type II neurons are small, bipolar, or pseudounipolar cells representing 5-10% of the total SGNs population, with their peripheral processes forming synapses with multiple outer hair cells [OHCs, 15, 16]. Usually, neither their cell bodies nor their processes have myelin cover [17]. IHCs and type I SGNs transduce most of all auditory input into the brain, while the OHCs amplify auditory input [15].
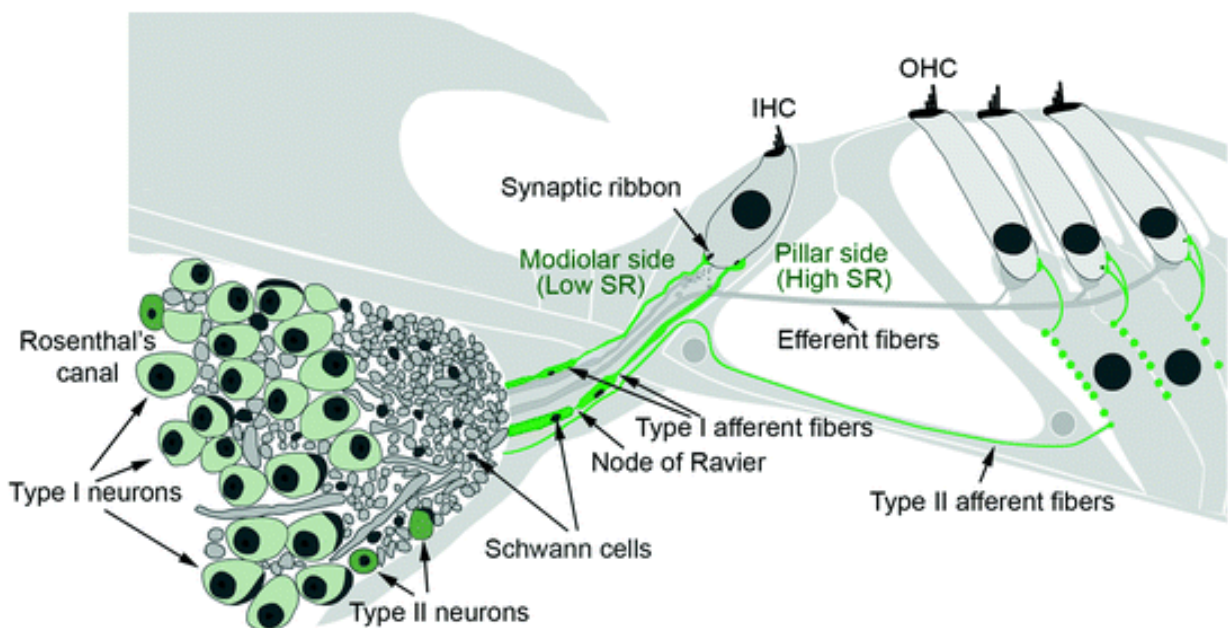
Figure 2. Schematic representation of the relationships between afferent and efferent auditory nerve fibers with two types of sensory hair cells (adapted from Dabdoub *et al*, 2015). SGNs are clustered in Rosenthal's canal (RC) and include two types of neuronal cells: large type I neurons that make up 90-95% of the SGN population and form synapses with inner hair cells (IHCs) and small type II neurons comprising 5-10% of the SGN population and innervating outer hair cells (OHCs). Type I nerve fibers are surrounded by myelinating Schwann cells, whereas type II nerve fibers are enclosed by nonmyelinating Schwann cells.

1.3 Tonotopy of the spiral ganglion neurons

The spatial separation of complex sounds based on frequency is known as tonotopy [15]. In mammals, the apex of the cochlea is tuned to low-frequency sounds, whereas the basal region responds to high-frequency sounds [1, 15, 17]. Spiral ganglion neurons also display frequency-dependent features and morphological variation along the tonotopic axis, such as a decrease in soma and axon size in the apical region [1, 15]. Neurons from the basal side showed significantly more rapid action potential latency and onset time course at the threshold than apical neurons [1], and the action potential duration was prolonged in the apex compared to the base [1]. Neurons from the base are rapidly accommodating neurons (RA) and mainly fire only a single action potential in response to prolonged depolarizing stimulation, whereas those from the apex are more slowly accommodating neurons (SA) with a broader range of accommodation profiles [1]. These kinetic differences can be explained by the differential distribution of potassium (K^+) channels in SGNs: base is more enriched with the voltage-gated K^+ channels, $K_v1.1$ and $K_v3.1$, and the large conductance calcium-activated potassium channel (BK); whereas apex is more enriched with the $K_v4.2$, a channel type that could contribute to the more prolonged action potential latencies at threshold [1, 15]. SGN action potentials were shown to depend on voltage-gated calcium channels, and antibody staining indicated that $Ca_v3.1$ and $Ca_v3.3$ are distributed in a clear tonotopic gradient with enrichment in basal SGNs [15].

1.4 Electrophysiologically relevant morphological specializations of spiral ganglion neurons

Type I neurons, which compose up to 95% of the ganglion, make one-to-one synaptic connections with inner hair cells (IHCs) receptors and are unique because of their bipolar configuration, in which the soma is part of the conduction pathway [1]. In many species, the soma of type I SGNs, composing the VIIIth cranial nerve, has a unique form of myelin, termed loose myelin [1, 18], whereas soma is unmyelinated in humans [1, 19]. Because of this, in the spiral ganglion, the action potential is initiated in the type I neurons proximal to the sensory receptors and transmitted along the axonal segment, which is intercepted by a large expanse of the soma membrane [1, 20]. Thus, the configuration of these neurons is unlike that of a typical neuron form a central nervous system, in which electrical input is received in the dendrites and integrated at the soma before generating an action potential at the spike initiation zone [1]. The electrophysiological significance of the soma is compounded by the fact that soma size are graded along the cochlear contour, where neurons in the apex are significantly smaller than those in the base [1, 19]. The bipolar spiral ganglion soma has multiple morphological specializations, such as the close proximity of surrounding nodes and differential diameter of its central versus peripheral initial processes that

counteract "branch failures", which would impede action potential conduction into the central nervous system [1, 20]. There is also evidence that soma is electro-genic and potentially capable of integrating signals as well as conducting them [1, 21]. In support of this evidence, microtubule-associated protein 2 (MAP2), a marker of dendrites and somatic integration region [1, 22], and a related protein CASPR, known to flank the nodes of Ranvier and found within the spike initiation zone [1, 20], have been localized in the soma of spiral ganglion neurons, along with multiple types of voltage-gated ion currents [1, 15, 17].

1.5 Neurotrophins

Neurotrophins and their receptors are crucial for the maintenance of inner ear innervation [1]. Neurotrophic factor neurotrophin-3-NT-3 is crucial for SGN survival during development [23, 24] and is postnatally expressed in the outer hair cells, with the highest levels in inner hair cells and adjacent supporting cells [23, 25]. Many studies have shown that NT-3 supports SGN survival *in vitro* [23, 26, 27] and *in vivo* after hair loss [23, 28, 29]. Brain-derived neurotrophic factor-BDNF is expressed at low levels in the outer hair cells at all ages and conditions [23]. Like NT-3, BDNF promotes SGN survival *in vitro* and *in vivo* [23, 26, 27], but its expression declines postnatally [23, 30]. Glial cell line-derived neurotrophic factor-GDNF is expressed in the cochlea and has been shown to provide trophic support to SGNs, support SGN survival *in vitro* [23, 31, 32] and *in vivo* [23, 32], and increases survival and neurite extension of SGNs [3].

1.6 Spiral ganglion neurons and topographical cues

In principle, neurites may respond to electrical, chemical, or topographical cues specifically designed to guide and orient them toward targets. For example, several *in vitro* studies show the effect of structured surfaces on cellular morphology and development [33-37]. Either anisotropic (fibers, grooves) or isotropic (pillars, holes) substrate induces topographic stimuli and affects neuronal morphology [33, 36, 37, 38-41]. Three previous studies investigated the effect of methacrylate with micro-grooves (anisotropic substrate) on SGN guidance [42, 43, 44]. Another study with adult rat SGN showed that microscale surface topographic features direct the growth of SGN neurites on photopolymerized microfeatures (anisotropic substrate) [45]. However, controlled guidance and patterned growth of the auditory neurons to form intimate contact with stimulating electrodes remain elusive. One of the models, the so-called "passive model"- silicon micro-pillar substrates (MPS), is composed of biocompatible material with surfaces proven to control neuronal growth and morphology *in vitro* [33-37, 46]. Studies with isolated SGNs [36, 46] and with isolated dorsal root ganglion neurons [37] demonstrated the capacity of micro-pillar substrates to support normal neuronal growth, enhance neurite alignment, promote outgrowth,

and induce specific morphologies on micro-pillars. Furthermore, several recent attempts to embed microelectrodes into multi-electrode arrays (MEA) using complementary metal–oxide–semiconductor (CMOS) technology yield promising results [47-51]. MPS can attract and guide spiral ganglion neurons but cannot ensure long-term neuronal survival due to the absence of electrical stimulation. *In vivo* studies have demonstrated that electrical stimulation from CI electrodes promotes the survival of SGNs [52, 53]. In contrast, MPS is a "passive substrate" containing only pillars and cannot provide information on the effect of the micro-electrodes' position. Thus, a step further from MPSs is an "active model," which is a substrate incorporating CMOS with the potential to stimulate neurons and record their electrical activity simultaneously. In this study, we developed and used CMOS chip substrates consisting of protruding pillars and pillar-like titanium nitride (TiN) micro-electrodes between 1.4 and 4.8 µm in diameter and with a spacing between 0.8 and 1.6 µm with a height of 1 µm. These dimensions are similar to typical mammalian cell bodies [47-49]. Furthermore, these micro-electrodes incorporate *in situ* circuits for voltage and current stimulation with an amplification transistor, all embedded in a silicon oxide environment.

1.7 Methods for measuring neuronal activity

1.7.1 Microelectrode arrays (MEAs)

Complementary semiconductor-metal-oxide (CMOS) technology is a powerful technology that can be more or less directly interfaced with electrogenic cells, like heart or brain cells *in vitro* [50]. For this purpose, the cells are cultured at the top of the CMOS chips, and during electrical activity in the cell, ions may flow quickly across the cell membrane within milliseconds. In such a way, an electric field is generated by moving ions and can be recorded by means of metal microelectrodes [50, 54, 55, 56]. Such extracellular recordings are noninvasive (no cell membrane puncturing), enabling long-term measurements [50]. The CMOS chips do not leak out toxic compounds, so the cells remain viable for extended periods [50]. Measurements at different points in the array were enabled by organizing many microelectrodes in the same array [50]. Voltage transients can be either applied by means of electrodes or stimulation spots, which then evoke depolarization of the nearby cell membrane and generate subsequent electrical cell activity [50]. A stimulation spot is a large, several-micrometer spot of either metal or dielectric material with a high dielectric constant connected to an electrical source through which stimulation signals are streaming [50, 57, 58]. The significant improvements of CMOS technology include 1) connectivity; on-chip multiplexing architectures can address large numbers of electrodes, 2) signal quality; the signal is conditioned right at the electrode by means of dedicated circuitry units

(filters and amplifiers), 3) ease of handling and use; many functions can be programmed or automated via user-friendly software and digital interfaces that directly address digital registers and logic or memory units on the chip side [50]. For MEAs, tissue slices, which are recorded immediately after being removed from the animal, or cell cultures (dissociated cell cultures or organotypic tissue cultures) can be used. Dissociated cultures represent cells with in vivo positions no longer preserved, whereas organotypic tissue cultures are slices maintained in vitro over time [50]. There are few factors to consider when recording with a MEA. First, the cell-electrode interface must be organized in a such wayto allow a close fit of the cells and electrodes on the chip, maximizing the signal-to-noise ratio [50]. Second, MEA chips are usually coated with cell-adhesion substrates such as poly-D-lysine, laminin, collagen, or fibronectin to promote cell or tissue attachment. [50, 59, 60]. Furthermore, a perfusion system is usually necessary for providing cells with the carbon gas and nutrients required to sustain the physiologic processes of the cells [50]. MEAs which is integrated into the substrate enable the study of neuronal information processing or the characterization of cellular responses upon dosing biologically active agents [50].

1.7.2 Patch-clamp

Patch-clamping represents a gold standard in the electrophysiology that offers detailed insight into the electrical properties of neurons [61]. It employs a glass micropipette which tightly adheres to the cell membrane, establishing a high giga-ohm seal resistance between them [61]. This setup allows for the observation of individual ion channels within a small section of membrane enclosed by the pipette tip in what is known as the cell-attached configuration [61]. By applying pressure to rupture this tiny membrane section, the electrode can access the cell's interior. This is termed the whole-cell configuration, permitting direct recordings of trans-membrane voltage and currents [61]. This method yields precise data about a cell's electrophysiological properties and the currents of individual ion channels [50]. However, it does have limitations: it's invasive, restricts cell viability duration, and the total number of cells examined concurrently is limited [50].

1.7.3 Calcium imaging

Calcium imaging, a technique where cells are loaded with calcium indicator dye, has been an important technique for neuroscientists because it has revolutionized the approaches for functional analyses in the living brains of animal experimental models [62, 63]. In all organ systems, Ca2+ is a ubiquitous intracellular messenger that regulates multiple cellular functions such as secretion, contraction, cellular excitability and gene expression [64]. Changes in intracellular calcium concentration $[Ca^{2+}]_i$ are strictly linked to the electrical activity in neurons and produce signals that can be effectively detected by optical methods [62]. Because of Ca^{2+}

ubiquitous nature, the Ca^{2+} indicators that would enable optical measurements of Ca^{2+} concentration in the cytoplasm of cells were developed [64]. The most commonly used fluorimetric calcium indicators are Fura-2, Fluo-3, Fluo-4, Aequorin, Rhod-2, Calcium green-1[64]. The advantages of fluorescence-based calcium imaging are its high temporal resolution in the millisecond range and its high spatial resolution in the micrometer range [62].

2. GOALS AND HYPOTHESIS

2.1 Goals

The main goal of this research is to obtain successful and viable *in vitro* cultures of spiral ganglion neurons (SGNs) grown on a high complementary-metal-oxide semiconductor electrode array (thereafter CMOS chip), which serves as a novel technological platform for future neuro-electronic devices. Morphological and electrophysiological characterization of *in vitro* SGN cultures are used to assess the biological environment of a CMOS chip containing 16,384 electrodes embedded with micro-pillars. The research has the following objectives:

- Morphological analysis of *in vitro* cultured spiral ganglion neurons on high complementary-metal-oxide semiconductor electrode array (CMOS chip);
- Electrical stimulation and recording of the electrical activity of spiral ganglion neurons using a high-density CMOS MEA chip;
- Comparison of the standard patch-clamp technique with the CMOS technology (advantages and disadvantages);

2.2 Hypothesis

The main hypothesis of this research is to assess whether a high-density complementary-metal-oxide semiconductor electrode array (CMOS) provides a favorable biological environment for the culturing and growing spiral ganglion neurons *in vitro* by demonstrating their viable morphological and electrophysiological properties.

3. MATERIALS AND METHODS

Material:

Chemical	Manufacturer
Neurobasal-A	Gibco, Thermo Fisher Scientific
DMEM	Gibco, Thermo Fisher Scientific
Fetal bovine serum (FBS)	Sigma Aldrich
Bovine serum albumin (BSA)	Sigma Aldrich
Trypsin-EDTA	Sigma Aldrich
DNAse	Sigma Aldrich
B27 Supplement	Gibco, Thermo Fisher Scientific
Glial cell line-derived neurotrophic factor (GDNF)	Milipore
Brain-derived neurotrophic factor (BDNF)	Milipore
Neurotrophin-3 (NT-3)	Milipore
L-glutamine	Milipore
Penicilin/Streptomicin	Lonza
Normal Goat serum	Dako
Mouse monoclonal anti-ßIII-tubuline (Tuj) primary antibody	Milipore
Rabbit polyclonal anti-S100 primary antibody	Sigma Aldrich, Milipore

Rabbit polyclonal anti-peripherin	Milipore
Alexa 568 goat anti mouse secondary antibody	Life Technologies
Alexa 488 goat anti-rabbit secondary antibody	Life Technologies
DAPI	Molecular probes

3.1. Experimental animals

SGNs were isolated from 5 to 7-day-old rat pups (*Rattus norvegicus*, females, breed Sprague-Dawley) and adult guinea pigs (*Cavia porcellus*, male and female, 350-430 g, breed Dunkin-Hartley). Animals were raised in animal housing under the following conditions:

- Ventilation: fresh air (15-20 changes per hour)
- Temperature: $22 \pm 2°C$
- Moisture: $55 \pm 10\%$, not under 30% and over 70%
- Light: diffuse lighting, 300 lobes, 1 m above the floor, 12 h day/night
- Food: pellets
- Water: sterile, fresh
- Bedding: comfortable and safe for adults and offspring, without dust, hypoallergenic

3.2. Methods

3.2.1 Preparation of CMOS chips and glass coverslips

In this study, we used the CMOS chip with the design, fabrication, and specifications reported by Huys *et al* [51]. Briefly, the 0.18 µm TSCM platform technology was used to create probe-card wafers consisting of a field dielectric layer of 400 nm SiO2 and one aluminum metal interconnect layer of 800 nm and 400 nm on top. The formation of three-dimensional structures with electrodes was supported by introducing vias and a layer of 100 nm TiN coating as well as by etching the oxide layer around the electrodes; this procedure led to the construction of an 8x8 mm^2 chip array with 16,184 electrodes with individual addressability for electrical stimulation and recording. Figure 3 shows the CMOS chip design together with scanning electron micrographs of superficial areas of an electrode array at different scales. Chips were grouped into two categories, depending on pillar widths. Narrow pillar widths were from 1.4 µm to 2.4 µm (1.4, 1.6, 2, and 2.4 µm), while wide pillar widths were from 2.8 µm to 4.8 µm (2.8, 3.2, 4 and 4.8 µm). Pillar spacing was from 0.8 µm to 1.6 µm (0.8, 1,

1.4 and 1.6 µm) and was equally distributed in areas of both narrow and wide pillars. Pillar height was kept constant at 1 µm. Chips were fabricated at imec vzw (Leuven, Belgium).

CMOS chips were cleaned overnight with acetone. All substrates were sterilized in 70% ethanol and coated with 0.01% poly-L-ornithine at room temperature overnight, cleaned with sterile water, and allowed to dry under sterile conditions. All samples were then placed in 24-well plates for testing.
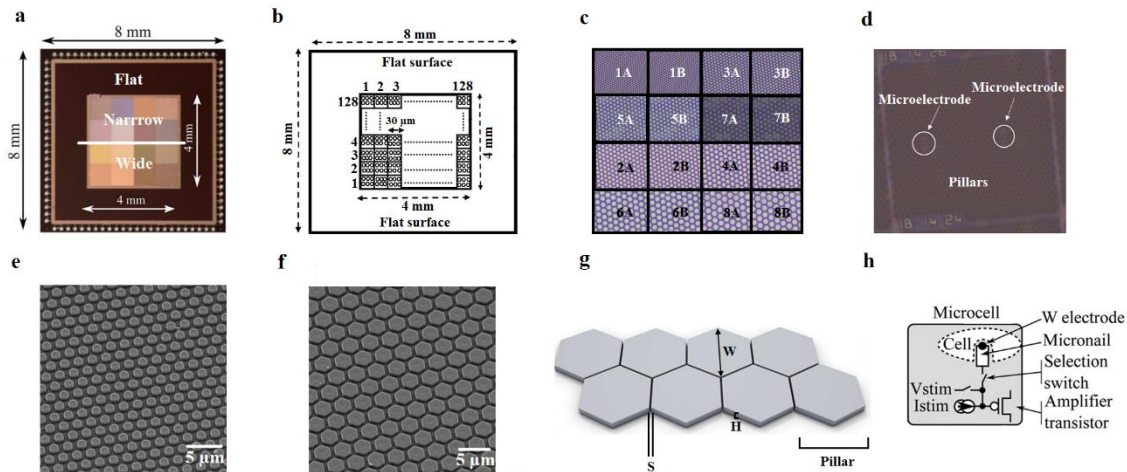
Figure 3. CMOS design (adapted from Radotić *et al*, 2018). **a)** Photograph of the CMOS chip. **b)** Chip sketch. The large active area of the CMOS chip measuring 4x4 mm consists of 128x128 addressable units called microcells. Each microcell is 30x30 µm and contains a local circuit and matrix of hexagonal micro-pillars (dummy pillars) and one active TiN micro-electrode for electrical stimulation and one recording TiN micro-electrode; **c)** Chip pillar areas with different pillar widths (white and black numbers). A and B pillar areas have the same properties, except that micro-electrodes in area A are nail-shaped, and micro-electrodes in B area are flat-shaped. Odd numbers (white, 1, 3, 5, and 7) are areas with narrow pillars: area 1: 1.4 µm; area 3: 1.6 µm; area 5: 2 µm and area 7: 2.4 µm, while even numbers (black, 2, 4, 6 and 8) are areas with wide pillars: area 2: 2.8 µm; area 4: 3.2 µm; area 6: 4 µm and area 8: 4.8 µm. The height of all pillars and electrodes is 1 µm, while spacing ranges from 0.8 to 1.6 µm (0.8, 1, 1.4, and 1.6 µm) for both narrow and wide pillars. **d)** Microphotograph of one microcell of the chip with micro-pillars and micro-electrodes (white circles with arrows). The scale bar is 100 µm; **e)** and **f)** The SEM images of the CMOS surface with narrow and wide pillars, respectively. The scale bar is 5 µm; **g)** Sketch of the pillars with W and H indicating the width and height of the pillar, respectively, while S indicates the spacing between pillars; **h)** One microcell of the chip is illustrated, containing the in situ circuits for voltage and current stimulation, an amplification transistor and the micro-nail electrode with cell position on the top of the electrode.

3.2.2 SGN isolation

Rat pups were placed on ice, anesthetized, and then decapitated. The dissecting buffer contained phosphate-buffered saline (PBS) supplemented with 0.3% bovine serum albumin (BSA) and 0.6% glucose. Under an operating microscope, the skull was opened along the mid-sagittal plane, and the brain was removed. The temporal bone was harvested and transferred to a clean dissecting buffer. The otic capsule was dissected, and the cochlea was identified and isolated. The organ of Corti and

modiolar cartilage were removed, and the spiral ganglia were collected in the dissecting buffer. Guinea pigs were anesthetized by intraperitoneal injection of ketamine (150 mg/kg) and xylazine (10 mg/kg) and then decapitated. The skull was bisected, and the brain was removed. The temporal bone was harvested and transferred to a clean dissecting buffer in such a way that it rested on the external acoustic meatus. The opening in the bulla was made using fine forceps, through which the rest of the roof of the middle ear cavity was removed with a pair of fine forceps. The bony cochlea appeared in view when the middle ear cavity was fully opened. The spiral lamina was isolated from the rest of the bony cochlea with delicate movements. The modiolus became exposed and separated from the rest of the temporal bone. Following its removal, the modiolus was broken up into several small pieces using fine forceps and collected in the dissecting buffer.

3.2.3 SGN cultivation

For dissociation, 500 µl of 0.25% trypsin-EDTA with the addition of 38 U/ml DNase was used. Dissociation was performed at 37°C for 30 minutes. The trypsinization was stopped by adding an equal volume (500 µl) of DMEM:F12 supplemented with 10% of Fetal Bovine Serum, also termed the STOP solution. For adult SGNs, the trypsinization was repeated twice for better dissociation. The tissue was then triturated, first with a 1000 µl pipette tip (gentle up and down suction for 20-25 times), followed by a 200 µl pipette tip (gentle suction for 20-25 times). Large pieces were allowed to settle down, and the cell suspension was collected. The cell suspension was then centrifuged for 5 minutes at 1000 rpm, and the pellet was resuspended in 500 µl of culture medium, which consisted of Neurobasal-A supplemented with 1% Pen/Strep, 0.25% L-Glutamine, 2% B27-supplement and 30 ng/ml GDNF. For the adult SGNs, centrifugation was performed for 5 minutes at 2000 rpm, and the pellet was resuspended in the same culture medium where two additional growth factors were added: 30 ng/ml BDNF and 30 ng/ml NT-3. Cells were counted using a Bürker-Türk chamber and seeded in a 100 µl volume at a density of 20,000 cells/well. Cells were allowed to settle down for 1-2h in the incubator (37°C, 5% CO_2, 85% humidity) when they were cultivated on glass coverslips and for 2-3h when they were cultivated on CMOS chips, after which the rest of the medium was carefully added to the well. Half of the medium was changed every 2-3 days.
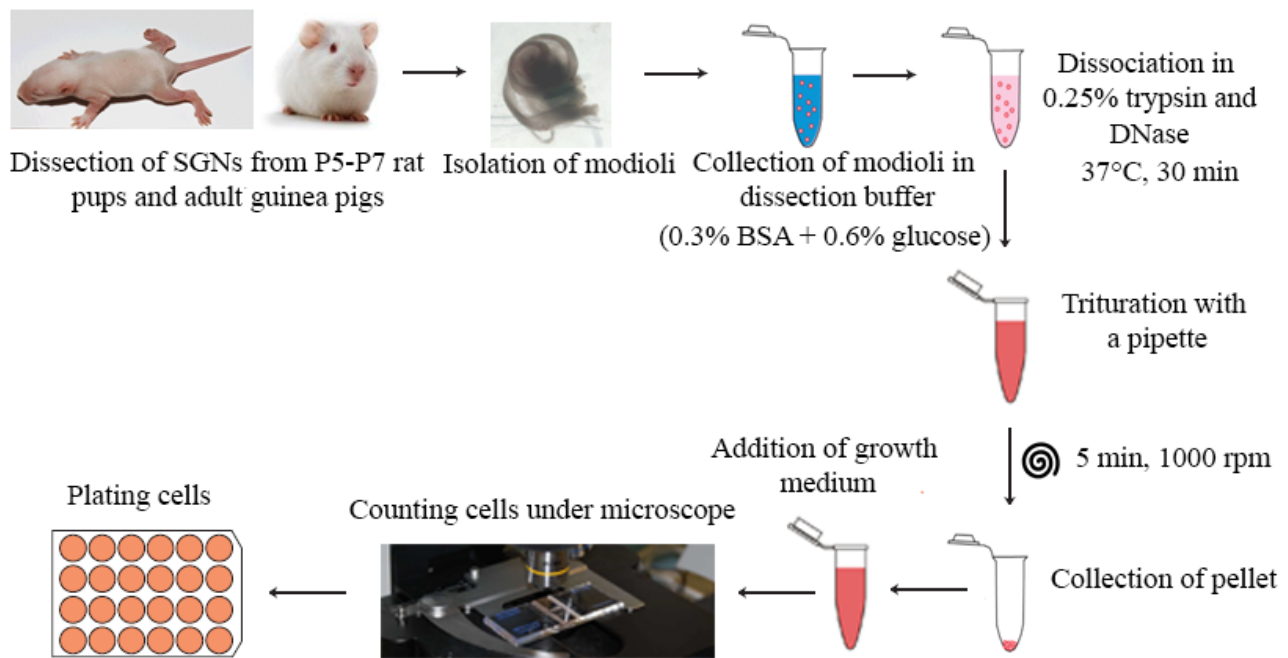
Figure 4. Culture protocol. Protocol for isolation and cultivation of spiral ganglion neurons

3.2.4 Immunocytochemistry, cell imaging and scanning electron microscopy (SEM)

SGNs were cultured during 1, 4, and 7 days *in vitro* (DIV) and fixed with 4% paraformaldehyde for 30 minutes. For immunocytochemical analyses, samples were washed three times with 0.01 M PBS, permeabilized with 0.1% Triton X-100 for 5 minutes, and blocked with PBS containing 1% normal goat serum for 90 minutes. The cells were then incubated in a dark humidity chamber overnight at 4 °C in PBS with 1% normal goat serum and mouse monoclonal anti-ßIII-tubuline (1:500) to stain neurons (named Tuj) and rabbit polyclonal anti-S100 (1:500) to stain glial cells. Rabbit polyclonal anti-peripherin (1:200) was combined with Tuj (1:500) to differentiate Type II SGNs from Type I SGNs in guinea pigs. On the next day, cells were washed three times with 0.01 M PBS, and incubated for 90 minutes at room temperature in PBS with 1% normal goat serum with Alexa 488 goat anti-mouse (1:500) and Alexa 568 goat anti-rabbit (1:500) secondary antibodies. At the end, DAPI in a ratio of 1:500 for 5 minutes was added. The samples were finally washed five more times with 0.01 M PBS and prepared for imaging with Immu-Mount. Imaging was carried out with the Olympus BX51 fluorescence microscope equipped with an Olympus DP71 camera. For SEM imaging, samples were fixed with 4% paraformaldehyde for 30 minutes, washed three times with 0.01 M PBS, followed by washing three times in distilled water (5-10 min each time) and immersing in increasing concentrations of ethanol (steps: 25% EtOH for 5 min; 50% EtOH for 10 min; 70% EtOH for 10 min; 96% EtOH for 10 min and 100% EtOH for 10 min, three times) and then brought to the critical point

of drying under airflow. A sputter coat of a thin layer of Au on top of the samples was added prior to SEM. Samples were visualized with an MIRA3 scanning electron microscope.

3.2.5 Presence and survival rate of SGNs

Given that the geometry of surface pillars exerts influence on *in vitro* grown neuronal cultures, the presence and survival rates of SGNs on CMOS were analyzed across three types of areas depending on micro-pillar widths: the narrow pillar CMOS group ("Narrow") contains neurons grown in areas with narrow pillars (1.4-2.4 µm), the wide pillar CMOS group ("Wide") have neurons grown in areas with wide pillars (2.8-4.8 µm) whereas the flat CMOS group ("Flat") contains neurons grown in areas of CMOS with no pillars. The number of SGNs for each experiment was calculated for each CMOS group, and then the SGN presence on glass coverslips and CMOS chips was assessed and compared between different CMOS groups and a control. In order to quantify the total neuronal cell number, Tuj+ cells were counted under the microscope on each sample, and the numbers were converted into cell densities representing the relative number of cells per mm^2 with areas normalized by sample surface areas (8 mm^2 for each area of a CMOS chip with micro-pillars, 132 mm^2 for a control glass coverslip and 48 mm^2 for the flat surface of the CMOS chip). The survival rate was calculated using the ratio of glial cells/neurons and the number of SGN/sample and is given as a percentage of the initial number of seeded cells per experiment, which was set as 100%.

3.2.6 Morphometric analysis of SGN

To describe the effect of the CMOS chip on SGN morphology, we carried out the analysis with ImageJ software (version 1.49, NIH, Bethesda, US). We focused on the following parameters: the neurite length and interaction with glial cells, the number of sprouting, and neuronal alignment, each described in the following sections.

3.2.7 Neurite length and interaction with glial cells

A large network of axons and dendrites of spiral ganglion neurons are non-specifically referred to as neurites when grown in culture [3, 6, 12, 17, 65, 66]. The average neurite length was described as a function of time (1 DIV, 4 DIV, and 7 DIV), and as a function of different CMOS chip areas (Narrow, Wide, or Flat). Neuronal cultures seeded and grown on glass coverslips represented a control. Neurites of every SGN were taken into account, and their length was measured by submitting fluorescent images into ImageJ and analyzed with a Simple neurite tracer plugin (Longair MH, Baker DA, Armstrong JD. Simple Neurite Tracer: Open Source software for reconstruction, visualization and analysis of neuronal processes. *Bioinformatics* 2011). The values were then represented in graphs with standard deviation bars. In addition, we assessed the interaction between SGNs with S100+ (glial) cells by direct overlapping or contact, both on CMOS chips and in control samples, as a

function of time (1 DIV, 4 DIV, and 7 DIV). We defined two categories: SGNs having neurites in overlap/contact with S100+ glial cells and SGN neurites not touching S100+ glial cells. The S100+/SGN ratio and the number of neurites of SGNs in contact with S100+ glial cells were counted manually in fluorescent, double-stained images.

3.2.8 SGN sprouting and morphology

The sprouting and its relation to neuronal morphology were determined on CMOS chips and the control glass coverslips as a function of time (1 DIV, 4 DIV, and 7 DIV). The morphological features were analyzed in accordance with previous work [17, 65, 66]. The number of neurites was scored visually in images for each Tuj+ cell to determine which neurons were neurite-free, mono-, bi-, multi-, or pseudo-unipolar. We did not count cells that were not clearly identified or were in clumps. The percentages of different morphologies were calculated from the total number of counted neurons.

3.2.9 Neuronal alignment

SGN alignment on control glass coverslips and CMOS chips was quantified using the ImageJ Fast Fourier Transform (FFT) Oval Profile plugin (authored by Bill O'Connell, https://imagej.nih.gov/ij/plugins/oval-profile.html), as previously described [67, 68, 69]. Briefly, 8-bit grayscale images of Tuj+ cells with a radial feather mask were created in Adobe Photoshop CS6 software (Adobe Systems Incorporated, San Jose, US), and then processed with the FFT function of the ImageJ software. The directionality of the objects in the resulting images depends on the intensity and distribution of the pixels. The Oval profile plugin performed the sum of the pixel intensities for 360 radii around the center of the FFT image. A straight line from the center to the edge of the FFT image (at angle θ) quantifies the objects oriented in that direction. The directionality of the original image is represented in plots of the sum of pixel intensities along angle θ. Images with no alignment showed constant pixel intensities across all angles, while peaks along one specific direction represented an image with pixels preferentially aligned in that direction [67, 68, 69]. The values (pixel intensities) from the analyses of the orientation of each neuron were averaged between neurons and plotted in the figure between 0° and 180° because the FFT decomposition is symmetrical around the horizontal axis and pixel summation between 180° and 360° is unnecessary.

3.2.10 Analysis of neurite width asymmetry

In each CMOS sample, we identified neurons with bipolar morphology to be analyzed for neurite width asymmetry with the following procedure: first, we submitted SEM images consisting of neurons with clear bipolar morphology into ImageJ. Then, the diameter of the soma was estimated for each identified bipolar neuron. Finally, the width of each neurite ("central" and "peripheral")

emanating from the soma was measured from the soma center at a distance corresponding to three times the diameter of the soma. This procedure was repeated for every bipolar SGN identified.

3.2.11 Electrical stimulation set-up and live Fluo-4-AM calcium imaging

The electrical stimulation set-up consisted of a custom-printed circuit board connecting the PC and the CMOS electrode array. The electrical connections of the chip were sealed with a biocompatible epoxy glue (Epotek 353ND, Epoxy Technology, Inc., Billerica, Massachusetts, US). Stimulation train pulse protocols were made in the Clampex software (version 10, Molecular Devices, LLC, San Jose, California, US) and consisted of short biphasic voltage pulses [48], each with a duration of 10 µs and voltage of 1.45V. Cells were loaded with the calcium dye Fluo-4 AM (Invitrogen, Belgium) to be able to monitor the changes in the intracellular calcium concentration ($[Ca^{2+}]_i$) when cells responded to electrical stimulation. The fluorescent marker Fluo-4 AM (Invitrogen, Belgium) was brought into the cells by ester loading. The final bath concentration was 5 µg/ml. The accurate position of potentially responsive SGN cells was identified by visual inspection, and we chose the closest electrode directly touching either the soma or neurite of the neuron to deliver stimulus pulse trains consisting of 10 pulses. Relative fluorescent changes in the intracellular calcium concentration ($[Ca^{2+}]_i$) were measured using 494 nm excitation and 516 nm emission filters of an upright Examiner microscope (Carl Zeiss, Belgium) equipped with a Hamamatsu cooled CCD camera. The fluorescent changes were measured as $\Delta F/F_{base}$, the change in fluorescence intensity relative to the baseline fluorescence intensity (F_{base}) prior to each stimulation train.

3. 2.12. Electrical recordings using CMOS-like multi-electrode-array chips

We performed neurophysiological experiments with CMOS-like multi-electrode-array chips at imec vzw (Leuven, Belgium). We used neurochips, labeled as HearME chips, that were designed and developed within the STRIPMED project at the University of Split, led by PI Damir Kovačić (Faculty of Science, University of Split). Chips were fabricated at imec vzw using a similar fabrication process described in Huys *et al* 2012 and Braeken *et al* 2012. These neurochips have 4 rows of electrodes, with each row consisting of 96 electrodes, arranged in 4 rows of 24 electrodes. Only 60 electrodes were selected for connection due to the spatial and wire-bonding constraints, with 30 electrodes on the top (Electrode row 1) and the other 30 on the bottom (Electrode row 4). On the CMOS-MEA chip, a glass ring was glued on the printed circuit board (PCB) around the CMOS chip using biocompatible epoxy for electrical isolation. The CMOS-MEA were then sterilized and coated as follows. After wiping the entire PCB surface with 70% EtOH, the active area of the CMOS chip was sterilized by filing the glass ring with 70% EtOH and let to stay for 20 min at room temperature. After 3 rinsing steps with sterile HPW (highly purified water), the chip was coated overnight at 37°C (incubator) using 50 µg/ml PDLO (poly-DL-ornithine, Sigma) dissolved in a borate buffer solution.

The next day, the chip surface was rinsed abundantly with sterile HPW, then coated with laminin (1 mg/ml) and let to stay for 2h at 37°C (incubator). Chip was washed 3 times with HPW and let to dry before culturing. The wire-bonded chips were packaged onto individual PCBs. Electrical connections were sealed with a biocompatible epoxy. A small ring was mounted on top of the carrier to hold the culture medium. Before starting experiments, the impedance of the chip was measured. Primary cultures of spiral ganglion neurons were prepared as described in Section 3.2.3. All the electrical measurements on the primary spiral ganglion neurons were performed at 37°C. First, we recorded for 1 min to allow the system to stabilize. After 1 min of recording, either spontaneous activity was recorded for 5 min from all electrodes by pressing on the record button of the software, or the amplitude/duration/shape of the stimulus was selected for stimulation. A biphasic (positive first) stimulus with a total duration of 60 μs and amplitude of 500 nA or 800 nA was used for stimulation. After applying stimulation, the activity of the neurons was recorded for 5 min. In neurons, electrical activity is always accompanied by an influx of Ca^{2+} ions. Thus, calcium imaging was used to monitor the electrical activity of SGNs cultured on glass coverslips and MEA chips. Fluo-4AM (Invitrogen, Belgium) was a calcium indicator and was brought into the cells by ester loading. Changes in the intracellular calcium concentration were observed with an upright Examiner microscope (Carl Zeiss, Belgium) equipped with a cooled CCD camera (Hamamatsu). Samples for fluorescent imaging were prepared as previously described in section 3.2.4. All the fluorescent images were taken using a confocal microscope (Zeiss Laser Scanning Microscope, LSM 780). The extracellular action potential (EAP) spatial distribution of a neuron was reconstructed using spike sorting algorithms (MC_Rack, MultiChannel Systems, Germany).
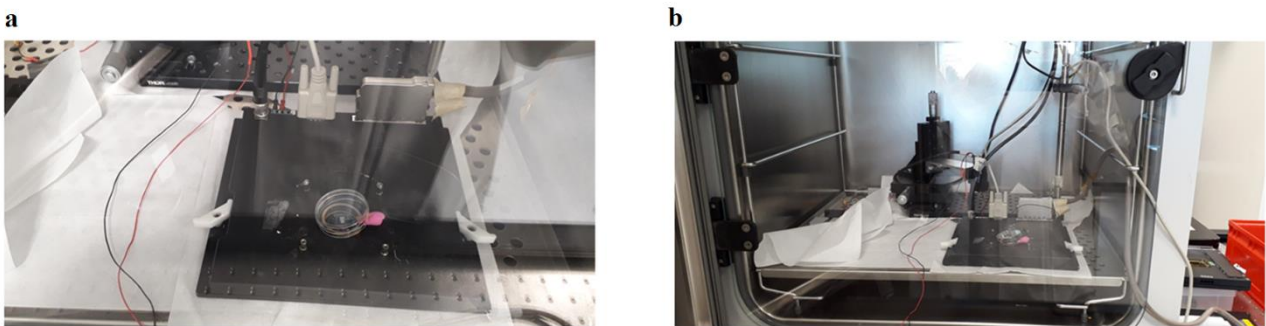
Figure 5. Cell cultures and stimulation set-up. a) One of the chips with SGN culture on PCB and stimulation set-up. **b**) Chip with SGN culture on PCB and stimulation set-up in the incubator.

3. 2.13. Statistical analysis

For statistical analysis, the Gaussian distribution was assumed, and data were transferred to spreadsheets and analyzed with MedCalc (version 15.2, MedCalc Software, Ostend, Belgium) and Sigmaplot (version 12.5, Systat Software, Inc., San Jose, US). The Shapiro-Wilk test, used to test the normality of the data distribution, confirmed a parametric distribution. For the comparison of the two groups, we used the Student's t-test. We performed multiple comparison analyses with one-way ANOVA, followed by a Tukey post-hoc test. Data are shown as mean ± standard deviation (SD). We considered a P value of less than 0.05 as significant. Significance was labeled as not significant, ns, ($P > 0.05$); *, +, # ($P < 0.05$); **, ++, ## ($P < 0.01$) and ***, +++, ### ($P < 0.001$). The confidence interval limits were defined with a probability of 95%.

4. RESULTS

1.1 4.1 Morphological characterization of spiral ganglion neurons on CMOS-MEA

4.1.1 CMOS chip is a favorable environment for the growth of neonatal and adult SGNs

Figure 6 and Figure 7 show an overview of the SGNs of neonatal rat pups and adult guinea pig cell cultures, respectively, on a) glass coverslips and b) a CMOS chip. Visual examination shows that neurons and non-neural cells are present both in the control and on CMOS chips, with neurons growing neurites in both conditions (CMOS and control). Figure 6c shows significant differences in the average neuronal density of neonatal SGN between CMOS and control substrates. Neonatal SGN cultures on CMOS chip micro-patterned surfaces were 3-fold more dense than on control substrates (4.8 vs. 1.6 per mm^2 respectively, Student's t-test, $P < 0.001$, M = 3, N = 18 for Narrow and Wide CMOS groups. In addition, micro-patterned surfaces of CMOS chip also yielded a significantly higher density of neonatal SGNs compared to the flat zones of CMOS areas (5.1 vs. 3.2 per mm^2, one-way ANOVA, Tukey post-hoc test, $P < 0.001$, M = 3, N = 18). Figure 7d shows significant differences (one-way ANOVA, Tukey post-hoc test; $P < 0.001$) in the survival rates between neonatal SGN grown on the different areas of the CMOS chip (Narrow, Wide and Flat) and the control glass surfaces. Survival rates of SGNs grown on the Flat surfaces of the chip and glass coverslips were similar (9.8 ± 3.4% for control vs. 11.5 ± 5.4% for Flat areas after 4 DIV) and were significantly lower, almost halved, compared to SGNs grown on the Narrow and Wide areas of the chip (22.8 ± 6.1% for Narrow areas and 19.7 ± 6.9% for Wide areas after 4 DIV). At 7 DIV, both the control and the CMOS chips yielded somewhat lower survival rates than 4 DIV, with the Narrow and Wide areas of the CMOS showing a smaller decrease than the control (one-way ANOVA, Tukey post-hoc test, $P < 0.05$).
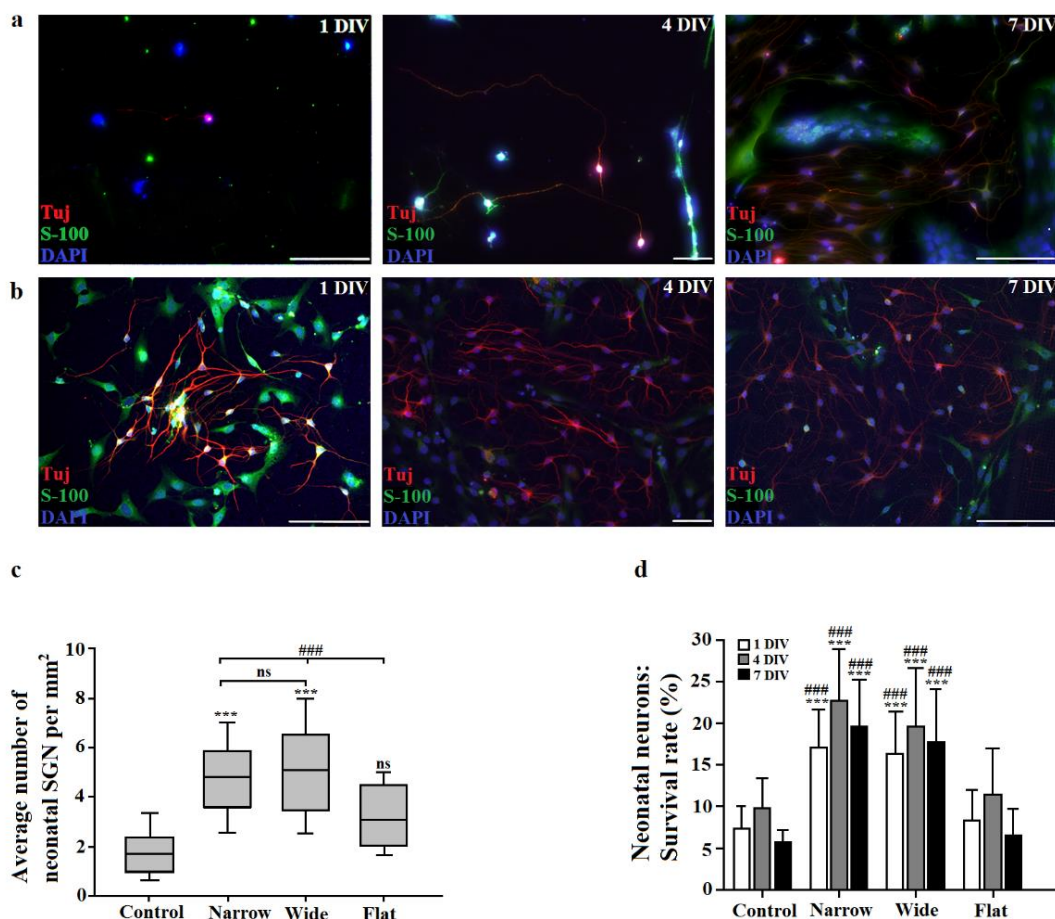
Figure 6. Presence of neonatal SGNs on glass coverslips (control) and CMOS chips (adapted from Radotić *et al*, 2018). Neurons stained with neuronal marker Tuj+ (red/magenta) and the nuclear marker DAPI (blue). Glial cells stained with glial marker S-100 (green) and nuclear marker DAPI (blue). **a)** SGNs on glass coverslips after 1 DIV, 4 DIV and 7 DIV. **b)** SGN on CMOS chips after 1 DIV, 4 DIV and 7 DIV. Scale bars: 200 μm **c)** Box and whisker plots showing an effect of CMOS chips on neonatal SGN density. * indicates differences to control: *** = P < 0.001 and ns = not significant (one-way ANOVA, Tukey post-hoc test), # indicates differences between area types: ### = P < 0.001 for the comparison between Narrow, Wide and Flat areas of the CMOS chip (one-way ANOVA, Tukey post-hoc test). **d)** Survival rate (%) of neonatal SGN on CMOS substrates and control glass coverslips. * indicates differences to control: *** = P < 0.001 (one-way ANOVA, Tukey post-hoc test) and # indicates differences of Narrow and Wide areas to Flat areas of the CMOS chip: ### = P < 0.001 (one-way ANOVA, Tukey post-hoc test).

Figure 7a and 7b show an overview of the adult SGN cell culture on (a) glass coverslips and (b) the CMOS chip. Fig. 8c shows significant differences in the average densities of adult SGNs grown on CMOS substrates compared to the control condition (one-way ANOVA, Tukey post-hoc test, P < 0.001). Adult SGN cultures on micro-patterned surfaces of the CMOS chip were about 2.4-fold more dense than cultures on glass coverslips (2.9 vs. 1.2 per mm^2 , respectively). Areas with wide pillars seem to additionally enhance SGN growth as maximal cell densities were obtained in these areas (Wide vs. Narrow areas, Student's t-test, P < 0.01, M = 3, N = 18). We also observed differences in the neuronal density between flat areas of CMOS chips (Flat area) and micro-patterned surfaces

(Narrow and Wide Zones grouped together), with Flat areas having a significantly lower density of adult SGN (2.5 vs. 1.7 per mm^2, one-way ANOVA, Tukey post-hoc test, $P < 0.001$, Figure 7c). Importantly, the control and flat areas of the CMOS chip were similar in terms of neuronal density for both neonatal and adult SGN (Fig. 7c and Fig. 8c). The control group yielded survival rates of $1.4 \pm 0.6\%$ after 1 DIV, $1.4 \pm 0.5\%$ after 4 DIV and $1 \pm 0.4\%$ after 7 DIV and were comparable with the survival rates of adult guinea pig SGN growing on the flat areas of the chip ($1.8 \pm 0.56\%$ after 1 DIV; $2 \pm 0.74\%$ after 4 DIV and $1.5 \pm 0.23\%$ after 7 DIV). Both were significantly lower from survival rates of SGN growing on the narrow and wide areas of the chip ($5.4 \pm 1.2\%$ after 1 DIV, $5.8 \pm 0.78\%$ after 4 DIV and $4.9 \pm 0.98\%$ after 7 DIV for Narrow, one-way ANOVA, Tukey post-hoc test; $P < 0.001$, and $7.1 \pm 2.3\%$ after 1 DIV, $7.9 \pm 1.7\%$ after 4 DIV and $6.8 \pm 1.6\%$ after 7 DIV for Wide, one-way ANOVA, Tukey post-hoc test; $P < 0.001$; Figure 7d). As for neonatal SGNs, the survival rates of adult SGN were decreased over time, and such a decrease was significantly lower on CMOS micro-patterned surface (Narrow and Wide) compared to the control (one-way ANOVA, Tukey post-hoc test, $P < 0.05$). When comparing neuronal densities across species, we found a significantly higher average density of neonatal SGNs compared to adult neurons (4.8 vs. 2.1 per mm^2, respectively).
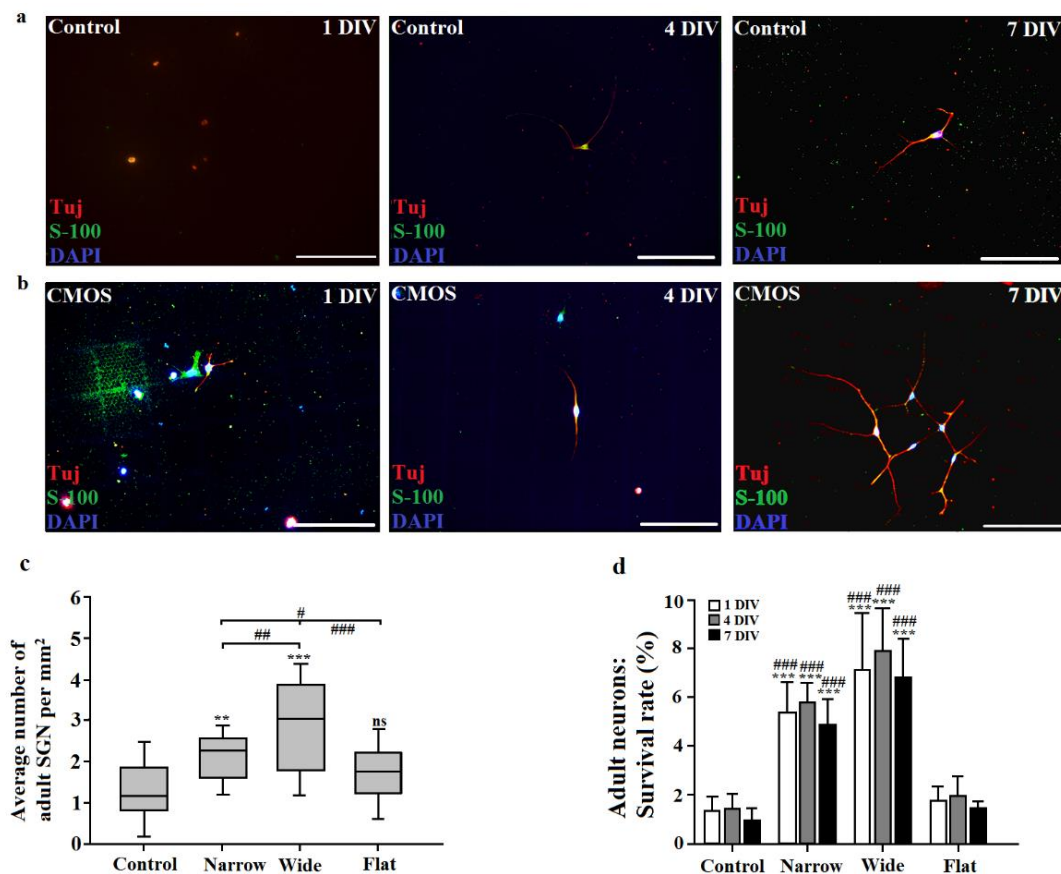
Figure 7. Presence of adult SGNs on glass coverslips (control) and CMOS chips (adapted from Radotić *et al*, 2018). Cells were stained with the neuronal marker Tuj (red/magenta), the glial marker S-100 (green), as well as with the nuclear marker DAPI (blue). **a)** Adult SGN on glass coverslips after 1 DIV, 4 DIV, and 7 DIV. **b)** Adult SGN on CMOS chips

after 1 DIV, 4 DIV, and 7 DIV. Scale bars: 200 μm **c)** Box and whisker plots showing an effect of CMOS chips on adult SGN density. * indicates differences to control: ** = P < 0.01, *** = P < 0.001 and ns = not significant (one-way ANOVA, Tukey post-hoc test), # indicates differences between Narrow, Wide and Flat areas of the CMOS chip: # = P < 0.05, ## = P < 0.01 and ### = P < 0.001 (one-way ANOVA, Tukey post-hoc test). **d)** Survival rate (%) of adult SGN on CMOS substrates and control glass coverslips. * indicates differences to control: *** = P < 0.001 (one-way ANOVA, Tukey post-hoc test) and # indicates differences between Narrow and Wide areas to Flat areas of the chip: ### = P < 0.001 (one-way ANOVA, Tukey post-hoc test).

4.1.2 CMOS substrates induce more bipolar and multipolar SGN morphology

The number of neurites sprouting from the SGN soma, producing neurite-free, pseudo-unipolar, monopolar, bipolar, and multipolar morphologies, determined the morphological shape of the SGN. As we did not observe any significant differences between the Narrow, Wide, and Flat areas of the CMOS chip regarding morphology, further comparisons were made between the control and the CMOS chip. Figure 8 shows the percentages of SGN neurons morphologically analyzed across time (columns), species (neonatal SGNs in the upper panel and the adult SGNs in the lower panel), and the area type (white bars for control and black bars for CMOS chips). Overall, bipolar neurons were the most abundant type for neonatal SGNs at all DIVs, as well as in the adults after 4 DIV. At 7 DIV, bipolar neurons were the most abundant type of neurons both in the CMOS and control conditions. Further analyses, detailed below, are performed depending on the polarity of the cells, separately for neonatal and adult neurons. First, neonatal neurite-free neurons were exceedingly more abundant in the control compared to CMOS ($35.6 \pm 15.9\%$ and $0.1 \pm 0.1\%$ at 1 DIV respectively, Student's t-test, $P < 0.001$; Figure 8a). After 4 DIV and 7 DIV, there were no neurite-free neurons on CMOS. On the control coverslips, the number of neurite-free neurons decreased to 4.5 ± 2.9 % after 4 DIV and to 3.8 ± 3.1 % after 7 DIV. Second, in the neonatal monopolar morphology, a dramatic effect of the CMOS was observed: after only 1 DIV, the CMOS chip produced just a few neonatal SGN neurons with a monopolar morphology ($1.2 \pm 0.8\%$) representing only 1/32 fraction of the value in the control condition ($38.7 \pm 15.1\%$), with similar findings at 4 DIV ($1.4 \pm 0.6\%$ on CMOS and $40 \pm 19.8\%$ on controls). After 7 DIV, percentages of monopolar neurons in the control condition was reduced by 7 times ($5.8 \pm 4.0\%$) compared to 4 DIV ($40.0 \pm 19.8\%$), and is approximately 7 times more abundant with respect to the CMOS ($0.8 \pm 0.47\%$). Third, the CMOS seems to have a strong opposite effect on neonatal bipolar morphology: at 1 DIV, CMOS produced 2.5 times more neonatal SGN ($64.6 \pm 13.6\%$) with respect to the control ($25.6 \pm 12\%$, Figure 8a-c). After 4 DIV, the percentages of bipolar neurons increased in control ($47 \pm 19.1\%$) and slightly decreased on the CMOS (58 ± 13.4 %), probably because the neurons developed other neurite(s) that transformed into multipolar type. Fourth, in contrast to mono- and bi- polar conditions, no multipolar neurons were present in the control condition after 1 DIV, while the CMOS produced a high number of multipolar neurons (32.4

24

± 13.3%). At 4 DIV, the percentage of neonatal multipolar SGN was still much higher on the CMOS (40.7 ± 14.9%), five times the number in the control condition (8.1 ± 3.6%, Figure 8a-c). However, with increasing DIVs, the percentages of multipolar SGNs increased particularly on control surfaces (23.6 ± 9.4% after 7 DIV), while the multipolar population on the CMOS remained reasonably stable (45.4 ± 18.9% after 7 DIV).

Regarding the morphology of SGNs in adult guinea pigs, neurite-free neurons were more abundant on control surfaces compared to the CMOS (86.6 ± 4.6% vs. 48.8 ± 10% after 1 DIV, 23.2 ± 5.6% vs. 4.9 ± 1.3% after 4 DIV and 14.8 ± 9.6% vs. 4.8 ± 2.3%, after 7 DIV, Figure 8d-f). There were no differences in the number of monopolar neurons at all DIVs between the control group and the CMOS (Figure 8d-f). Similar to the neonatal group, bipolar morphology on the CMOS was significantly more abundant with respect to the control group at all DIVs except 7 DIV: 35.1 ± 13.9% after 1 DIV, 70.5 ± 12.7% after 4 DIV and 52.5 ± 8.7% after 7 DIV compared to control with 5.2 ± 1.8% after 1 DIV, 54.2 ± 14.8 after 4 DIV and 53.9 ± 15.2% after 7 DIV. Similar to the neonatal neurons, no multipolar adult neurons after 1 DIV on control glass coverslips were observed, while on CMOS chips, 15.3 ± 4.2% of the adult SGN were of the multipolar type. At 4 DIV, the percentages of multipolar neurons on CMOS and control surfaces were similar (Figure 8d-f), with 7 DIV again showing more multipolar neurons on CMOS compared to the control. These results suggest that the CMOS environment dramatically influenced neuronal morphology, strongly favoring bipolar and multipolar morphology and, to a lesser extent, monopolar morphology in neonatal and adult spiral ganglion neurons.
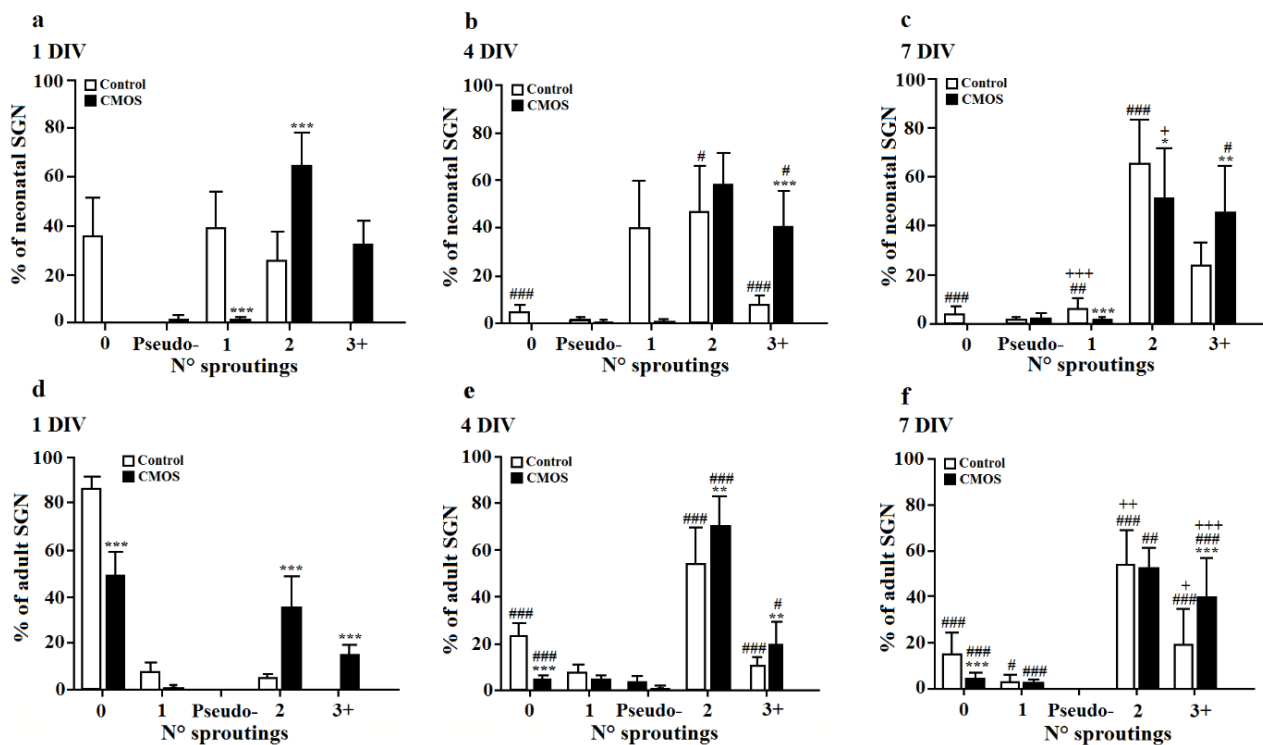
Figure 8. The effect of CMOS chip on neonatal and adult SGN neuronal morphology (adapted from Radotić *et al*, 2018). The upper row shows data for neonatal, the lower for adult SGN, while the columns separate data based on DIV time. **a)** Quantification of neonatal SGN neuronal morphology on control and chip substrates after 1 DIV, **b)** after 4 DIV, and **c)** after 7 DIV where N° indicates the number of sproutings (0 = neurite-free, 1 = monopolar, 2 = bipolar, 3+ = multipolar). Significant differences are indicated by # for differences by 1 DIV: # = P < 0.05, ## = P < 0.01, ### = P < 0.001 (one-way ANOVA, Tukey post-hoc test), by + for differences by 4 DIV: + = P < 0.05, ++ = P < 0.01 and +++ = P < 0.001 (one-way ANOVA, Tukey post-hoc test) and by * for differences between the control and CMOS substrates: * = P < 0.05; ** = P < 0.01, *** = P < 0.001 (Student's t-test). **d)** Quantification of adult SGN neuronal morphology on control and chip substrates after 1 DIV, **e)** after 4 DIV, and **f)** after 7 DIV. Significant differences are indicated by # for differences by 1 DIV: # = P < 0.05 and ### = P < 0.001 (one-way ANOVA, Tukey post-hoc test), by + for differences by 4 DIV: + = P < 0.05, ++ = P < 0.01 and +++ = P < 0.001 (one-way ANOVA, Tukey post-hoc test) and by * for differences between control and CMOS substrates: ** = P < 0.01, *** = P < 0.001 (Student's t-test).

4.1.3 CMOS micro-patterned surfaces induce neurite elongation and decrease neurite-glial cell interaction in neonatal and adult SGN.

Already after 1 DIV, the neurites of neonatal SGNs on the CMOS were 3.6 times longer compared to the control group (347.6 ± 115.5 μm vs. 95.6 ± 37 μm respectively, Student's t-test, P < 0.001, M = 3, N = 18, Figure 9a). The axon length was measured only at 1 DIV and 4 DIV for neonatal neurons, however, over time, the neurites from neonatal SGNs were found intertwined between each other. It was challenging to identify neurites belonging to the same cell somas. Nevertheless, in both conditions (CMOS and the control group), the neurites were significantly longer with more days *in vitro* (one-way ANOVA, Tukey post-hoc test, P < 0.001, Figure 9a), and the increase was more considerable for adult neurons. There were no significant differences in the neurite length between

neurons growing on narrow and wide areas of the CMOS chip for both neonatal and adult SGNs. However, the neurite length of neonatal and adult SGNs that were grown on the flat surface of the CMOS chip was similar to those on control surfaces (476.1 ± 101 µm vs. 480 ± 86.2 µm after 4 DIV for neonatal SGN and 90.4 ± 19 µm vs. 74.1 ± 16.2 after 4 DIV for adult SGNs respectively, one-way ANOVA, Tukey post-hoc test, $P > 0.05$, Figure 9a, b) and was significantly lower compared to the micro-patterned surfaces of the CMOS chip (one-way ANOVA, Tukey post-hoc test, $P < 0.001$, Figure 9b). Neonatal neurons had longer axons compared to adult neurons (580.1 ± 136.2 µm vs. 127 ± 17.7 µm at 4 DIV respectively). Previous observations of SGNs *in vitro* cell cultures demonstrated that these neurons often grow their neurites in contact with the S100+ cells, indicating glial type of cell [36, 70, 71], most probably Schwann and satellite cells [36, 72, 73]. For the neonatal SGNs, the ratio of glial cells/neurons was 2.3 ± 0.6 on the CMOS chips and 3.2 ± 0.9 for the control group after 4 DIV, 5.1 ± 1.2 (CMOS) vs. 8.6 ± 3.7 (control) after 7 DIV. For the adult SGNs, the ratio of glial cells/neurons was 2.6 ± 1.0 for the CMOS chips and 3.6 ± 1.3 for the control group after 4 DIV and 2.1 ± 0.7 (CMOS) vs. 2.9 ± 1.1 (control) after 7 DIV. Furthermore, we analyzed the interaction of a neurite from neonatal and adult SGNs with the S100+ cells after 1 DIV, 4 DIV, and 7 DIV for CMOS and control surfaces (Figure 9c, d). After 1 DIV, in the control group, $72.4 \pm 13.2\%$ of the neonatal SGN neurites and $37.6 \pm 9.1\%$ of the adult SGN neurites sprouting from the somas were in contact with the S100+ cells, which was not significantly different from the micro-patterned surfaces of the CMOS chip where $57.6 \pm 18.4\%$ of the neonatal neurites and $24.1 \pm 7.6\%$ of the adult neurites were touching the glial cells. (One-way ANOVA, Tukey post-hoc test, $P > 0.05$). After 4 DIV, in the control group, $67.4 \pm 14.6\%$ of the neurites sprouting from the neonatal SGN soma were in contact with the glial cells, while on the micro-patterned surfaces of the CMOS chip this percentage was almost three times lower ($22.9 \pm 5.1\%$ for Narrow Pillar areas and $26.7 \pm 9.7\%$ for Wide Pillar areas, one-way ANOVA, Tukey post-hoc test, $P < 0.001$). Adult SGNs growing on micro-patterned surfaces of the CMOS chip had $15.5 \pm 4.6\%$ (Narrow Pillar) and $14.1 \pm 5.8\%$ (Wide Pillar) neurites in contact with glial cells after 4 DIV, which was significantly lower compared to the control ($43.4 \pm 8.6\%$) and flat surface of the chip ($34.1 \pm 7.4\%$, one-way ANOVA, Tukey post-hoc test, $P < 0.001$). A similar outcome was also found after 7 DIV for adult SGNs, since neonatal neurons were challenging to analyze.
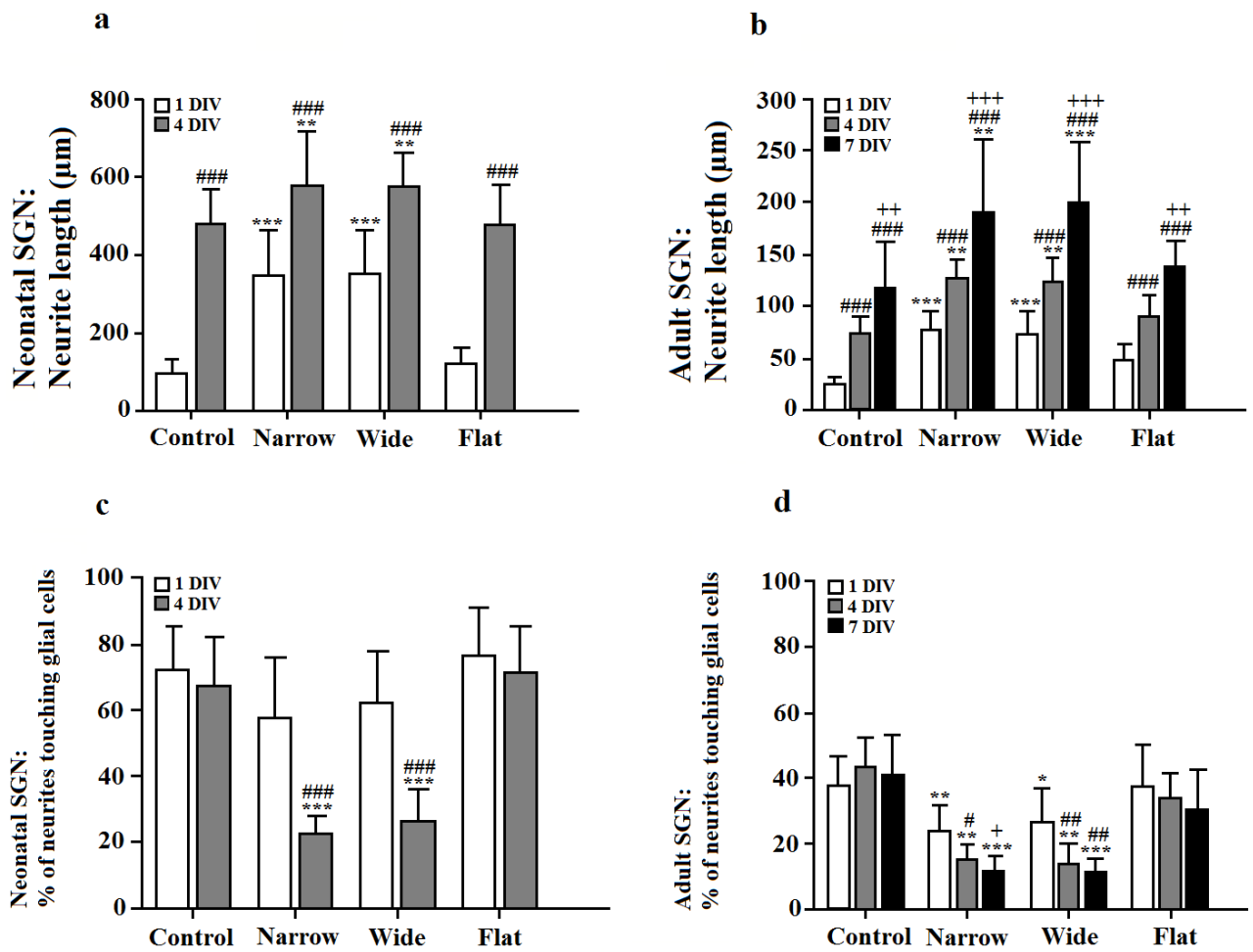
Figure 9. The effect of the CMOS area types on the neurite length and interaction with S100+ cells (adapted from Radotić *et al*, 2018). **a)** Bars and standard deviations show the distribution of neonatal SGN neurite length as a function of time. # indicates differences by 1 DIV: ### = P < 0.001 (Student's t-test) and * indicates differences to control: ** = P < 0.01, *** = P < 0.001 and ns = not significant (Student's t-test). **b)** Bars and standard deviations show the distribution of adult SGN neurite length as a function of time. # indicates differences by 1 DIV: ### = P < 0.001 (one-way ANOVA, Tukey post-hoc test), + indicates differences by 4 DIV: ++ = P < 0.01, +++ = P < 0.001 and * indicates differences to control: *** = P < 0.001 and ns = not significant (one-way ANOVA, Tukey post-hoc test). **c)** Quantification of the interaction of the neonatal SGN neurite with S100+ glial cells in the control condition and CMOS chips as a function of time. # indicates differences by 1 DIV: ### = P < 0.001 (Student's t-test) and * indicates differences to control: *** = P < 0.001 (Student's t-test). **d)** Quantification of the interaction of the adult SGN neurite with S100+ glial cells on control and CMOS chips. * indicates differences to control: * = P < 0.05, ** = P < 0.01, *** = P < 0.001 (one-way ANOVA, Tukey post-hoc test), # indicates differences by 1 DIV: # = P < 0.05 and ## = P < 0.01 (one-way ANOVA, Tukey post-hoc test) and + indicates differences by 4 DIV: + = 0.05 (one-way ANOVA, Tukey post-hoc test).

4.1.4 Specific CMOS topography elicits directional SGN neurite orientation and alignment.

In order to determine how micro-pillars dimensions (width and spacing) of the CMOS chips influenced the neurite orientation and alignment, we stained and visualized neonatal and adult SGNs grown on CMOS chips and glass coverslips with Tuj+ (Figure 10). The FFT Oval Profile analysis showed that the hexagonal topographical pattern of the pillars had a strong influence on the alignment and orientation of neurite outgrowth on CMOS micro-patterned surfaces (Figure 10b). On specific micro-patterns, neurites were shown to be preferentially oriented and aligned along three directional axes, spaced by 60° angle intervals (30°; 90°; 150°), closely following angles within a hexagon. On the other hand, the topographic guidance was instead reduced on glass coverslips (control) and flat areas of the chip (Figure 10a,c), suggesting that only specific topographic structures of the CMOS substrates provide mechanical support and guidance for growth and differentiation of SGNs. Pillar width was shown not to have an influence on neuronal alignment and orientation since the effect of pillar widths was similar in narrow and wide areas of the CMOS substrates.
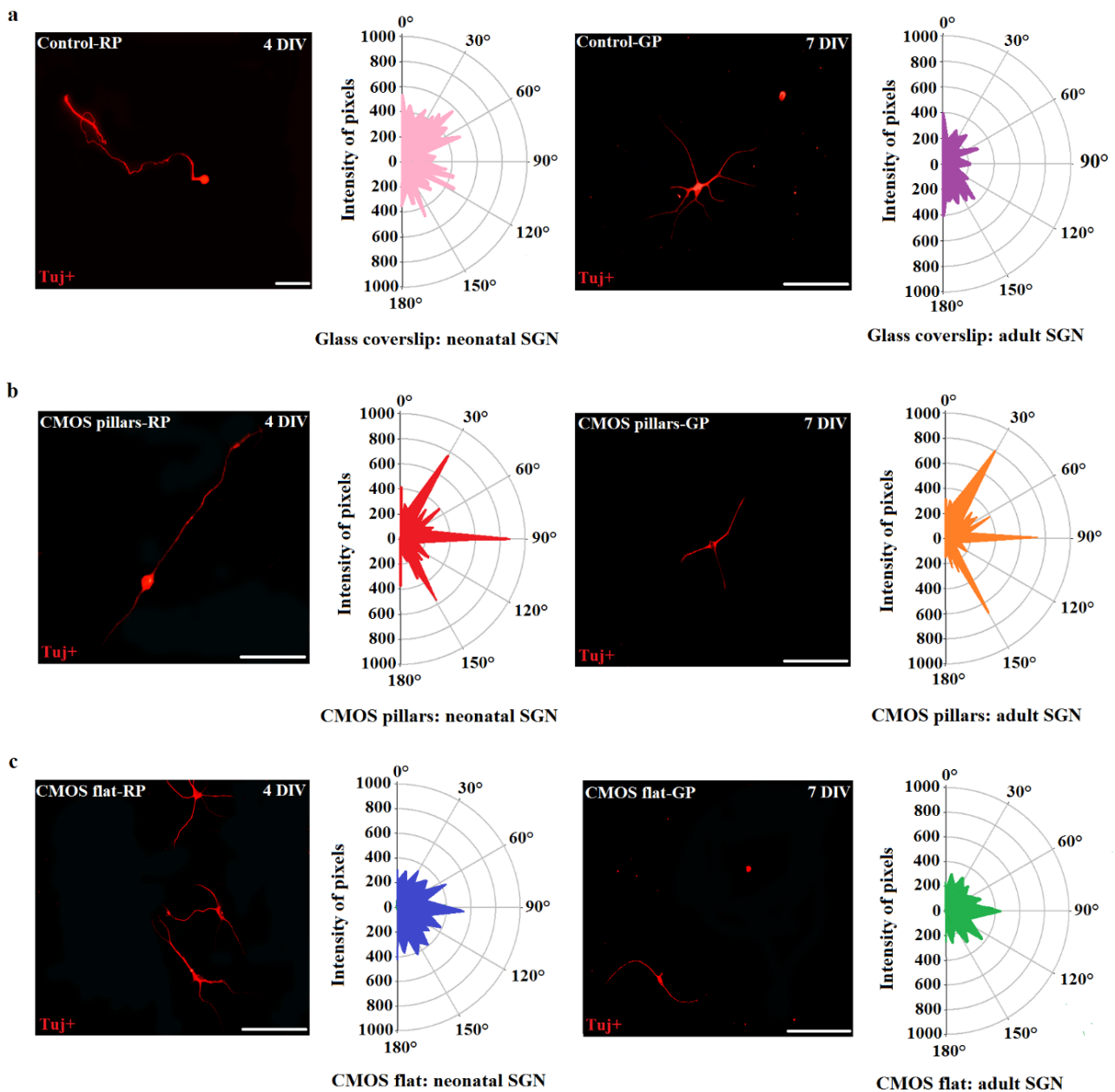
Figure 10. The effect of CMOS topography on neurite orientation and alignment (adapted from Radotić *et al*, 2018). Representative fluorescent images of Tuj+ neonatal and adult SGN alignment as well as alignment profiles of neurite growth around the preferred angles on glass coverslips **(a),** CMOS micro-patterned surfaces **(b),** and CMOS flat surfaces **(c)**. RP = rat pups, GP = guinea pigs. Scale bars: 200 μm. The radial values range from 0–1000, representing the intensity of pixels from FFT images along the same angle, while the angles are from 0 to 180 degrees. The values obtained by FFT Oval Profile picture analysis were averaged across neurons. For the control, 77 neonatal and 42 adult SGNs were analyzed. (N = 18), For CMOS micro-patterned surfaces, 203 neonatal and 162 adult SGNs were analyzed (N = 18) and for CMOS flat surfaces, 134 neonatal SGNs and 87 adult SGNs were analyzed (N = 18).

To visualize neurons growing on the CMOS areas with micro-patterned pillars, we obtained scanning electron images (SEM) of the spiral ganglion neurons after cultures were properly stained and prepared. Figure 11 shows the interaction of neurites with pillar structures and micro-electrodes.

Neurites grew in straight lines on top and between pillars in mostly a single direction with occasional perpendicular branching. Neurites on pillars also formed a nerve growth cone which filopodia utilize as anchoring points for axon repositioning when on the CMOS pillar.
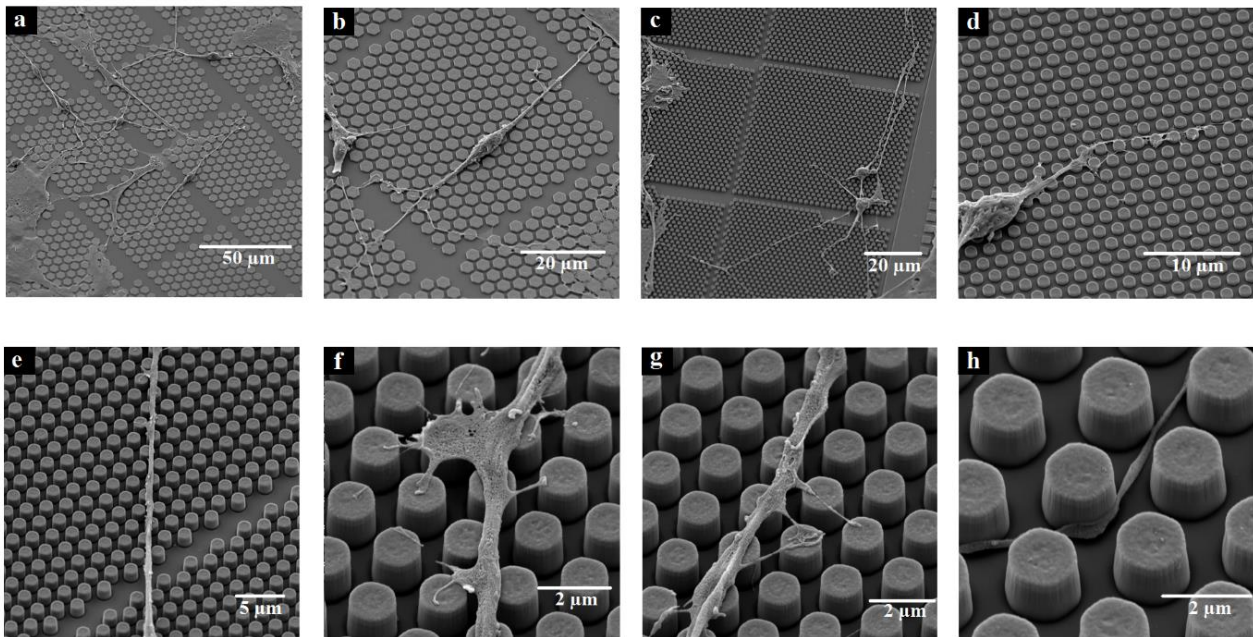
Figure 11. SEM images of spiral ganglion neurons cultured on CMOS chips (adapted from Radotić *et al*, 2018). **a)** SGNs cultured on CMOS chip. **b)** Bipolar neurons cultured on CMOS chip. Neurites grow in straight lines. **c)** Two neurons grow on top of the CMOS chips without the favorable flat surface of the chip. **d)** SGN cell soma with the neurite following micro-pillars on the CMOS chip. **e)** The neurite is guided by micro-patterned surface of the chip, follows a single angle determined by the spatial distribution of the pillars, and can cross a small divide of 2 μm without pillars between microcells (see Fig. 1) and attaches to the pillars on the other side of the divide; **f)** Growth cone formation on micro-pillars of the CMOS chips serves for axon repositioning; **g)** One neurite with protruding branches seeking interaction with pillars; **h)** one neurite passing between pillars showing how it touches pillars, probably in order to maintain the contact guidance.

4.1.5 CMOS topography promotes the growth of Type I and Type II of adult SGNs

Adult SGNs cultured on CMOS chips and glass coverslips were stained with rabbit polyclonal anti-peripherin to distinguish between Type I and Type II SGN. While there were no anti-peripherin positive neurons in the control condition, the CMOS substrates contained $3.3 \pm 1.9\%$ of neurons (n = 386, M=3, N=18), showing a strong positive effect for anti-peripherin (Figure 12b and 12c). The rest of the SGNs were not strongly positive for anti-peripherin and were identified as Type I SGNs (Figure 12a and 12c). The average diameter of somas from Type II SGNs was 11.4 ± 1.32 μm and was significantly smaller than the somas from Type I SGNs (23.6 ± 7.8 μm, Student's t-test, P < 0.001). The average length of a neurite was 137.9 ± 26.9 μm and was also significantly shorter than the length of a neurite from Type I SGNs (200.3 ± 56.7 μm, Student's t-test, P < 0.001).

Type II SGNs can be bipolar or pseudounipolar [16, 17]. In this study, mostly bipolar Type II SGNs appeared on the CMOS chip (Figure 12b).
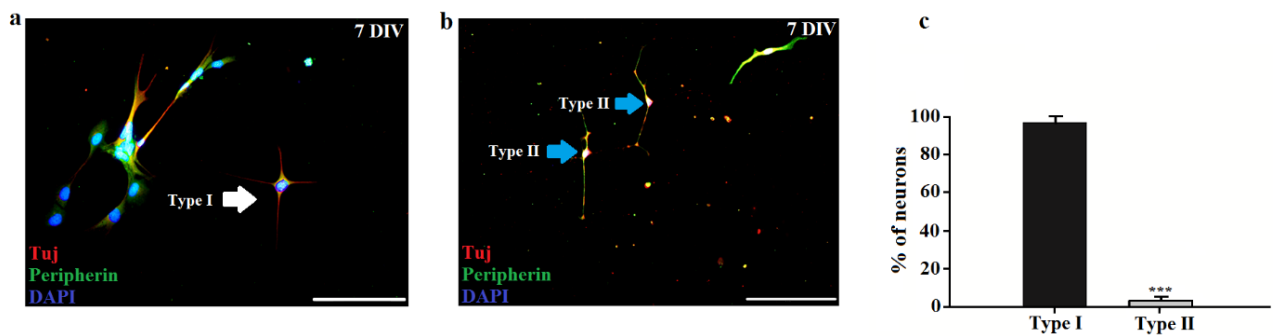
Figure 12. Presence of Type I and Type II of adult SGNs (adapted from Radotić *et al*, 2018) **a)** and **b)** Fluorescent images of guinea pigs type I and II SGNs on CMOS chips: Neurons stained with neuronal marker Tuj (red) and the nuclear marker DAPI (blue). Type II SGNs stained with peripherin (green) and the nuclear marker DAPI (blue). The white arrow shows Type I SGNs and the blue arrows show Type II SGNs from guinea pigs. Scale bars: 200 µm. **c)** Percentage of Type II SGNs from guinea pigs in comparison with Type I SGNs (M = 3, N = 18, n = 386). *** = P < 0.001 (Student's t-test).

4.1.6 Neurite width asymmetry

The bipolar spiral ganglion soma has multiple morphological specializations, such as the proximity to surrounding nodes and the differential diameter of its central versus peripheral neurite processes. This neurite width asymmetry presumably counteracts "branch failures" which, if unchecked, would ultimately impede action potential conduction towards the central nervous system. Thus, we analyzed neurite width asymmetry for each SGN with the bipolar morphology using SEM images providing clear neurite processes. Figure 13a demonstrates this phenomenon observed in the SEM image for neonatal SGNs cultured *in vitro* on the CMOS chip, showing two opposite neurite processes with differential widths; the wider one presumably represents the central process, and the thinner one indicates the peripheral process in accordance with the neuroanatomy of the SGNs. Measuring neurite width asymmetry in all neonatal SGNs with a bipolar morphology available on SEM images, we found significantly wider widths of one neurite process compared to the opposite neurite process (Figure 13b. the average width of the thinner process (peripheral process) was 0.41 ± 0.24 µm and that of the wider process was 0.85 ± 0.28 µm Student's t-test, P < 0.001, M = 1, N = 5, n = 24.
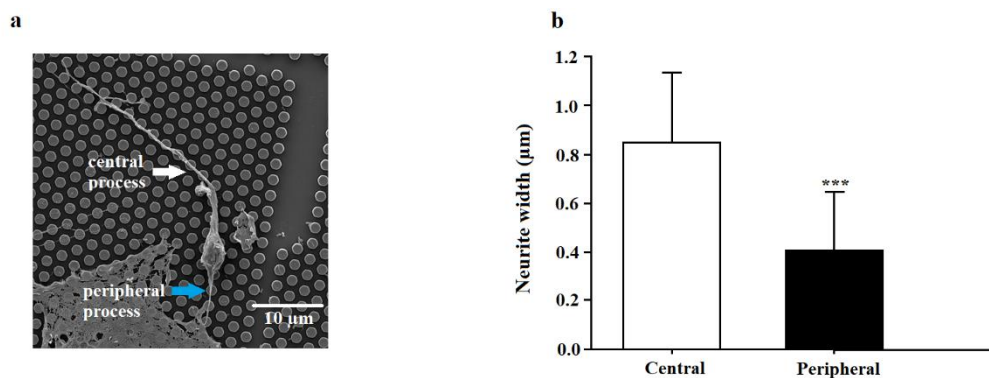
Figure 13. Neurite width asymmetry (adapted from Radotić *et al*, 2018). **a)** SEM image of a typical bipolar spiral ganglion neuron with its central and peripheral processes (white and blue arrow). **b)** Quantification of neurite width: * indicates a significant difference between central and peripheral processes width: *** = P < 0.001 (Student's t-test).

4.1.7 Micro-patterned surfaces of the CMOS chip demonstrate feasibility for normal neuronal growth without coating

To assess the extent of the advantageous environment of the micro-patterned surfaces with embedded electrodes for neuronal growth, we looked at whether non-coating of the substrate surfaces would be detrimental to neural growth. Specifically, we cultured SGNs on the CMOS chips without adding any coating chemicals (i.e., poly-L-ornithine), which is usually required for *in vitro* cultures. In our case, we found similar SGN presence on the chips with and without coating only on micro-patterned areas of the chips containing pillars and micro-electrodes (Figure 14a). On the other hand, neuronal density was significantly decreased on non-coated Flat areas of the chip compared to the same surface coated with poly-L-ornithine ($3.2 \pm 1.2\%$ on coated Flat areas of the CMOS vs. $0.97 \pm 0.44\%$ on non-coated Flat areas of the CMOS, Student's t-test, P < 0.001, M = 2, N = 12). Similar to neurons, the number of glial cells identified as S100 positive cells was also decreased on non-coated Flat areas of the CMOS chip. As for neurite length, we found that neurons express similar growth patterns on non-coated micro-patterned CMOS surfaces as on coated surfaces. No significant differences were found in neurite length for coated and non-coated CMOS micro-patterned surfaces (one-way ANOVA, Tukey post-hoc test, P > 0.05, M = 2, N = 12). However, there was a significant difference in neurite length between coated and non-coated Flat areas of the CMOS; neurites on non-coated flat surfaces of the CMOS chip were almost half the length (56.7 ± 19.2 μm) when compared to coated flat surfaces (123.3 ± 37.4) after 1 DIV and 2.5-fold shorter (189.4 ± 58.6 μm) after 4 DIV in comparison to coated flat surfaces (476.1 ± 101 μm). Neuronal alignment as well as interaction with glial cells and morphology, were similar on non-coated substrates as for coated substrates described above. In striking contrast with the micro-patterned CMOS surfaces, neuronal attachment to control glass coverslips without coating was negligible, demonstrating the necessity for substrate coating.

These results confirm that micro-patterned surfaces with embedded micro-electrodes of the CMOS chip represent a favorable environment for neuronal attachment and growth without coating chemicals.
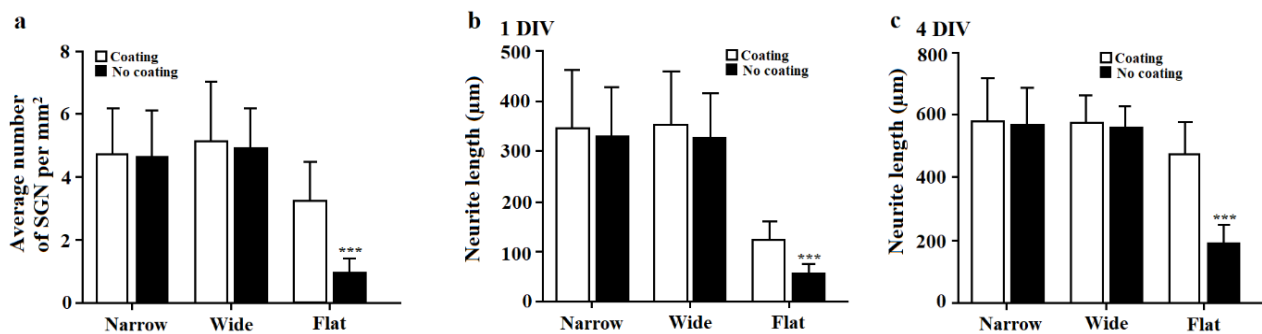
Figure 14. Influence of a substrate coating on neuronal presence and growth (adapted from Radotić *et al*, 2018). **a)** Bars and standard deviations showing an effect of substrate coating on SGN density. * indicates significant differences between coated and non-coated flat surfaces of the CMOS chip: *** = $P < 0.001$ (Student's t-test). Bars and standard deviations showing an effect of substrate coating on neurite length after **b)** 1 DIV and **c)** 4 DIV.* indicates differences between coated and non-coated flat surfaces of the CMOS chip: *** = $P < 0.001$ (Student's t-test)

4.1.8 Micro-patterned surfaces of the CMOS chip represent a favorable environment for electrophysiological applications

The position of the micro-electrodes on the chip and the spacing between pillars are parameters that affect electrophysiological measurements. Recordings of electrical activity and electrical stimulation on SGNs can presumably be performed if their soma lies directly on the top of a micro-electrode or if their neurites are in direct contact with a micro-electrode. Figure 15 shows that $28 \pm 8.7\%$ of the total neonatal SGNs growing on Narrow areas and $25.7 \pm 6.3\%$ of the total neonatal SGNs growing on Wide areas had their soma positioned on the top of a micro-electrode. Similarly, $23.9 \pm 7.6\%$ of the total adult SGNs growing on Wide pillars and $19.2 \pm 7.1\%$ of the total number of adult SGNs growing on Narrow areas had their soma positioned on the top of a micro-electrode. Comparing across species and CMOS areas, we found that only the Narrow areas of CMOS chips yielded a significantly higher number of neonatal SGNs with their soma residing on the top of the micro-electrode (Student's t-test, $P < 0.05$, M = 3, N = 18). Similar findings were observed within all days *in vitro* for both neonatal and adult SGNs. Expanding analyses with neurites going over the micro-electrode, we found that neonatal SGNs had $45.2 \pm 9.2\%$ of the total neurites growing on Narrow areas are in direct contact with a micro-electrode and $43.2 \pm 8.5\%$ of the total neurites have direct contact with a micro-electrode on Wide areas. Adult SGN had $32.7 \pm 8.3\%$ of the total neurites growing on Narrow areas being in direct contact with a micro-electrode and $36.7 \pm 7.5\%$ in the case of Wide pillars, which is significantly smaller compared to the neonatal SGNs on narrow pillars (Student's t-test, $P < 0.05$, M = 3, N = 18).

Similar results were confirmed for all days *in vitro* (Figure 15e-f). These results suggest that CMOS micro-patterned surfaces provide a favorable environment for the growth and alignment of neonatal and adult SGN and can also enable effective electrophysiological stimulation and recording.
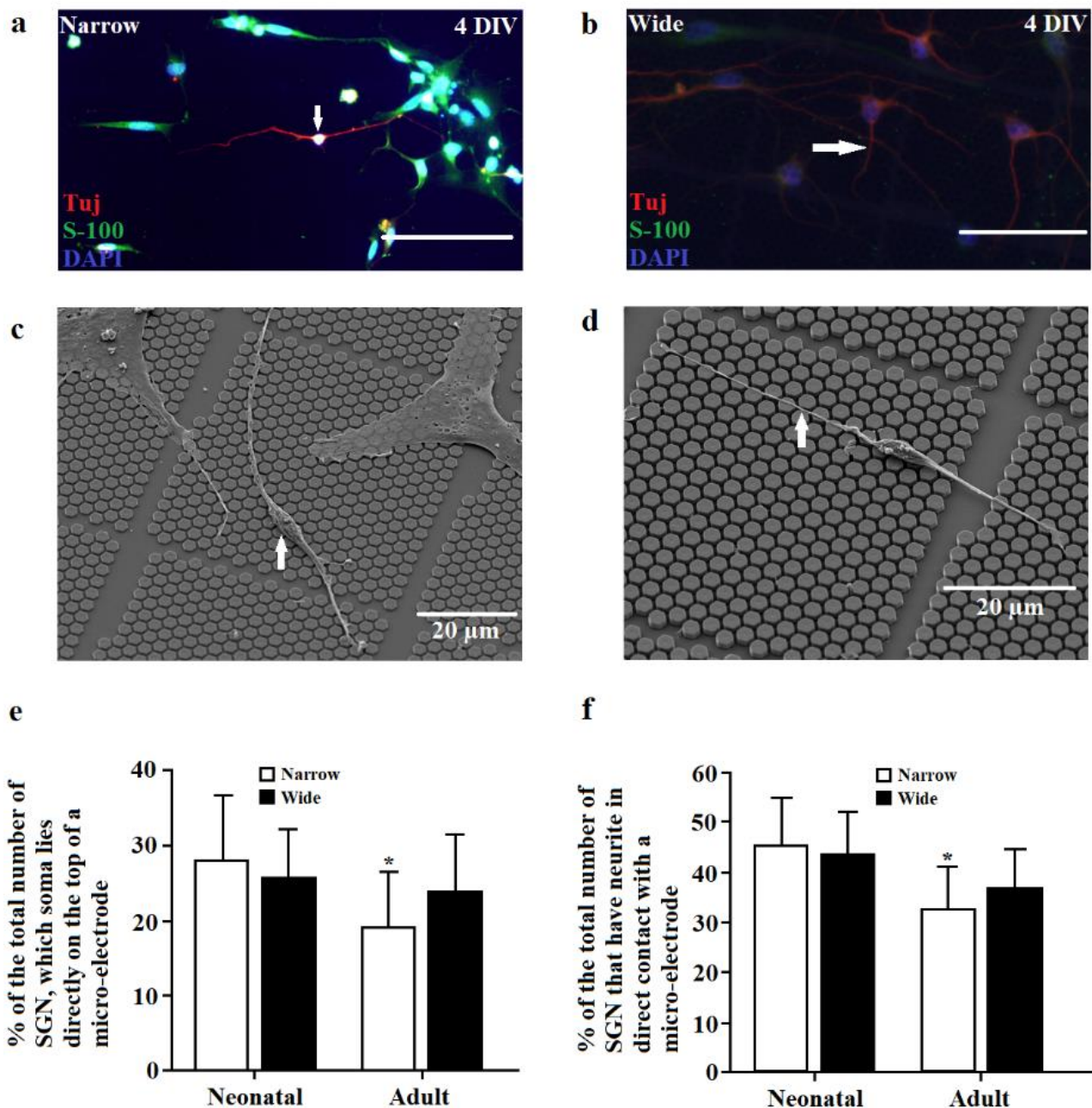
Figure 15. Contacts of the SGN soma and neurites with micro-electrodes (adapted from Radotić *et al*, 2018). **a)** Fluorescent image of a neonatal SGN with its soma being positioned directly on the top of a micro-electrode (white arrow). Cells were stained with the neuronal marker Tuj (red/magenta), glial marker S-100 (green), as well as with the nuclear marker DAPI (blue). Scale bar: 200 μm **b)** Fluorescent image of a neonatal SGN with a neurite spanning a micro-electrode (white arrow). Cells were stained with the neuronal marker Tuj (red/magenta), glial marker S-100 (green), as well as with the nuclear marker DAPI (blue). Scale bar: 200 μm **c)** SEM image of a neonatal SGN with its soma positioned directly on the top of a micro-electrode (white arrow). **d)** SEM image of a neonatal SGN with neurite spanning a micro-

electrode (white arrow). **e)** Quantification of neonatal and adult SGNs with their somas positioned directly on the top of a micro-electrode. * indicates a difference between neonatal and adult SGNs on narrow pillar area: * = P < 0.05 (Student's t-test). **f)** Quantification of neonatal and adult SGNs with neurites spanning a micro-electrode. * indicates difference between neonatal and SGNs on narrow pillar area: * = P < 0.05 (Student's t-test).

4.2 Electrophysiological recordings of spiral ganglion neurons on CMOS-MEA

4.2.1 The CMOS electrode array enables electrical stimulation of the SGNs-observation using Calcium imaging

We cultured spiral ganglion neurons for 6 DIV and 7 DIV on top of the CMOS electrode array chip to investigate the ability to stimulate SGNs electrically. Neurons were loaded with the calcium dye Fluo-4-AM to be able to monitor the changes in the intracellular calcium concentration ($[Ca^{2+}]_i$) of the SGNs close to the stimulation electrode. We selected a pair of electrodes that were located near or beneath the presumptive neuronal soma or neurite of the neuron and applied a train of biphasic pulses between electrodes. Stimulation pulses were applied through the electrodes while monitoring the changes in $[Ca^{2+}]_i$. Figure 16 shows a substantial increase in the relative $[Ca^{2+}]_i$ initiated in neurons whose soma lies directly on the top of a micro-electrode or whose neurites are in direct contact with a micro-electrode in response to electrical stimulation. Stimuli were trains of either 5 or 10 pulses, each with a duration of 10 µs and stimulation voltages of 1.45 V. In Figure 16a, we indicated three regions of interest (ROI 1, ROI 2 and ROI 3) along Fluo-4 calcium-stained spiral ganglion neurons and noticed that the signal of calcium fluorescent changes spread from neuronal soma along both neurites (Figure 16b, 16d). The same neuron was then stained with both the neuronal marker Tuj and glial marker S-100. The stimulated cell was positive only to Tuj, indicating the cell was indeed a spiral ganglion neuron (Figure 16c). Temporal dynamics of calcium imaging responses were similar in all five observed neurons (Figure 16e).
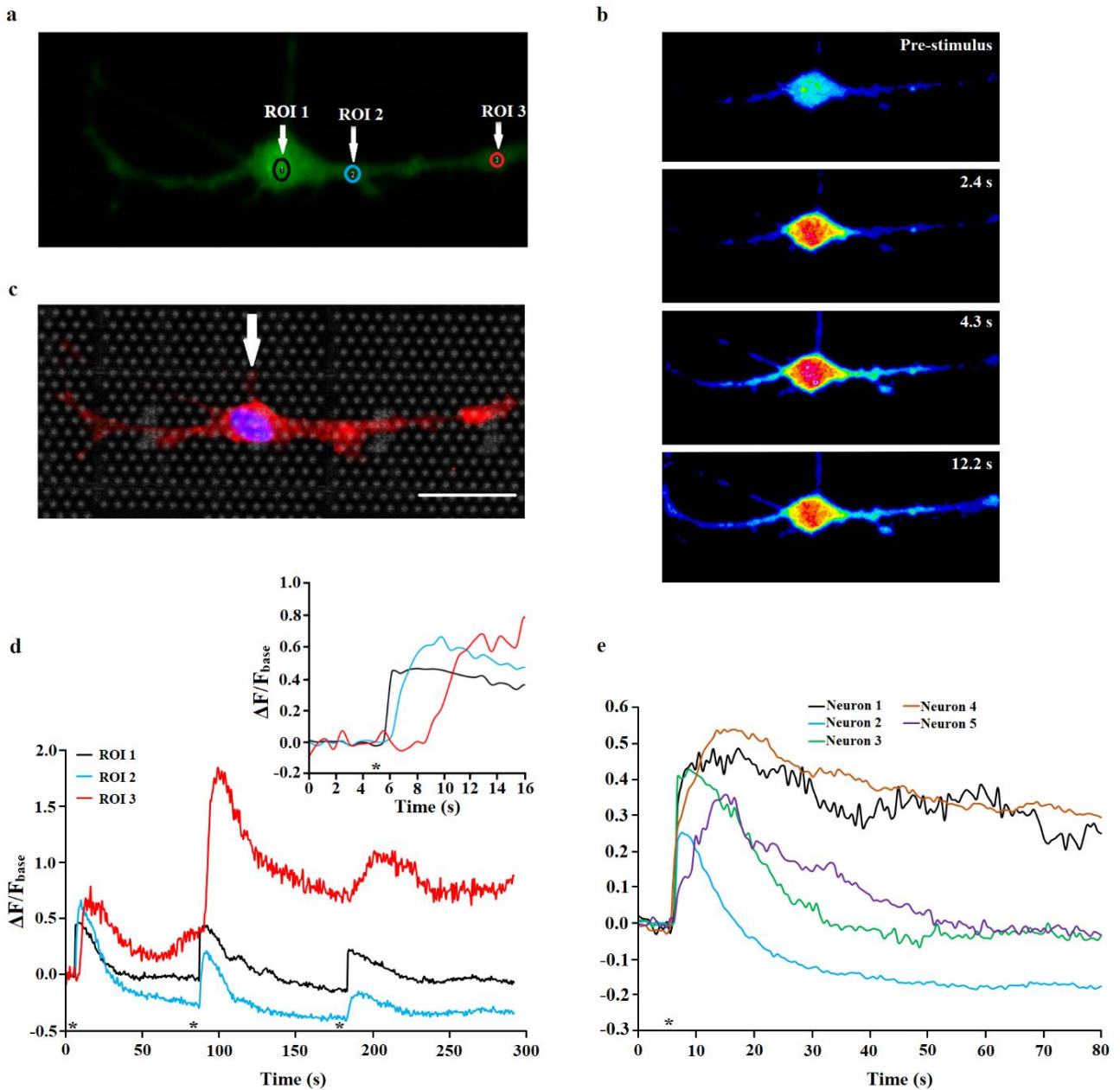
Figure 16. Fluo-4-AM calcium imaging and localized stimulation of SGN by biphasic electrical stimulation (adapted from Radotić *et al*, 2018). **a)** An image of a spiral ganglion neuron after Fluo4 calcium staining. The yellow circles indicate regions of interest (ROI 1, ROI 2, ROI 3). **b)** Time sequence of intracellular calcium concentration ($[Ca2+]i$) of a single SGN in response to electrical pulse train. The timing of the image capture is shown in the upper right corner and is relative to the stimulus onset. **c)** Fluorescent image of a spiral ganglion neuron stained with Tuj (neurons, red) and S-100 (glial cells, green). The stimulated cell was positive for neuronal marker Tuj only. The soma of the stimulated SGN lies directly on the top of the micro-electrode (white arrow). Scale bar: 25 µm. **d)** Relative changes in $[Ca^{2+}]_i$ in three regions of interest indicated in a) by circles with the corresponding color. The inset shows a magnification of the graph right after the first stimulation. * indicates the onset of the electrical pulse train. **e)** Relative changes in $[Ca^{2+}]_i$ in five observed neurons indicated with the corresponding color.

4.2.2 Electrophysiological recordings to investigate spontaneous and electrode stimulation-dependent activity

MEA electrodes can be used both to electrically stimulate neuronal cultures grown on the surfaces of the MEA neurochips as well as to record their electrophysiological activity. For stimulation, we used current sources delivering biphasic waveforms with a duration of 60 µs per phase at two signal amplitudes, 500 and 800 nA. Figure 17, 18, and 29 show representative raw voltage recording traces from primary spiral ganglion neurons at 7 DIV and 9 DIV on three HearMe chips. Both spontaneous activity and electrical activity after stimulation were recorded. Spiral ganglion neurons were prepared as described in section 3.2.3. All the electrical measurements on the primary spiral ganglion neurons were performed at 37°C. First, we recorded for 1 min to allow the system to stabilize. After 1 min of recording, either spontaneous activity was recorded for 5 min from all electrodes by pressing on the record button of the software, or the amplitude/duration/shape of the stimulus was selected for stimulation. A biphasic (positive first) stimulus with a total duration of 60 µs and amplitude of 500 nA or 800 nA was used for stimulation. After applying stimulation, the activity of the neurons was recorded for 5 min. All the fluorescent images were taken using a confocal microscope (Zeiss Laser Scanning Microscope, LSM 780). The extracellular action potential (EAP) spatial distribution of a neuron was reconstructed using spike sorting algorithms (MC_Rack, Multi Channel Systems, Germany).
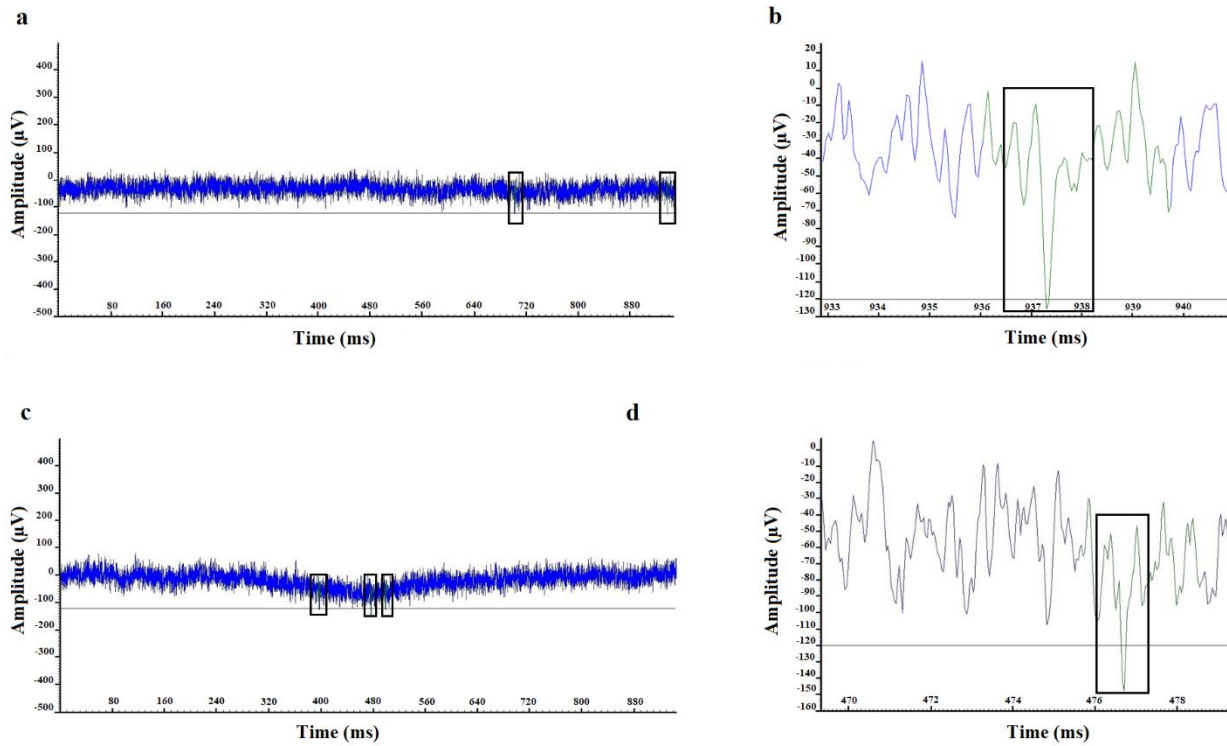
Figure 17. Spontaneous activity and neuronal voltages of the spiral ganglion neurons after stimulation from a chip HM-B10-X3 (stimulation after 60 s with current amplitude of 500nA, internal reference electrode). a) Raw traces of the recorded spontaneous electrical activity in the primary spiral ganglion neurons at 7 DIV unveiling individual spikes with an amplitude of 122µV and 126 µV; **b)** Profile of an individual spike with an amplitude of 126 µV corresponding to the second black rectangle in a; **c)** Raw traces of the recorded electrical activity in the primary spiral ganglion neurons at 7 DIV after stimulation unveiling individual spikes with an amplitude of 124, 148 and 124 µV; **d)** Profile of an individual spike with an amplitude of 148 µV corresponding to the second black rectangle in d.
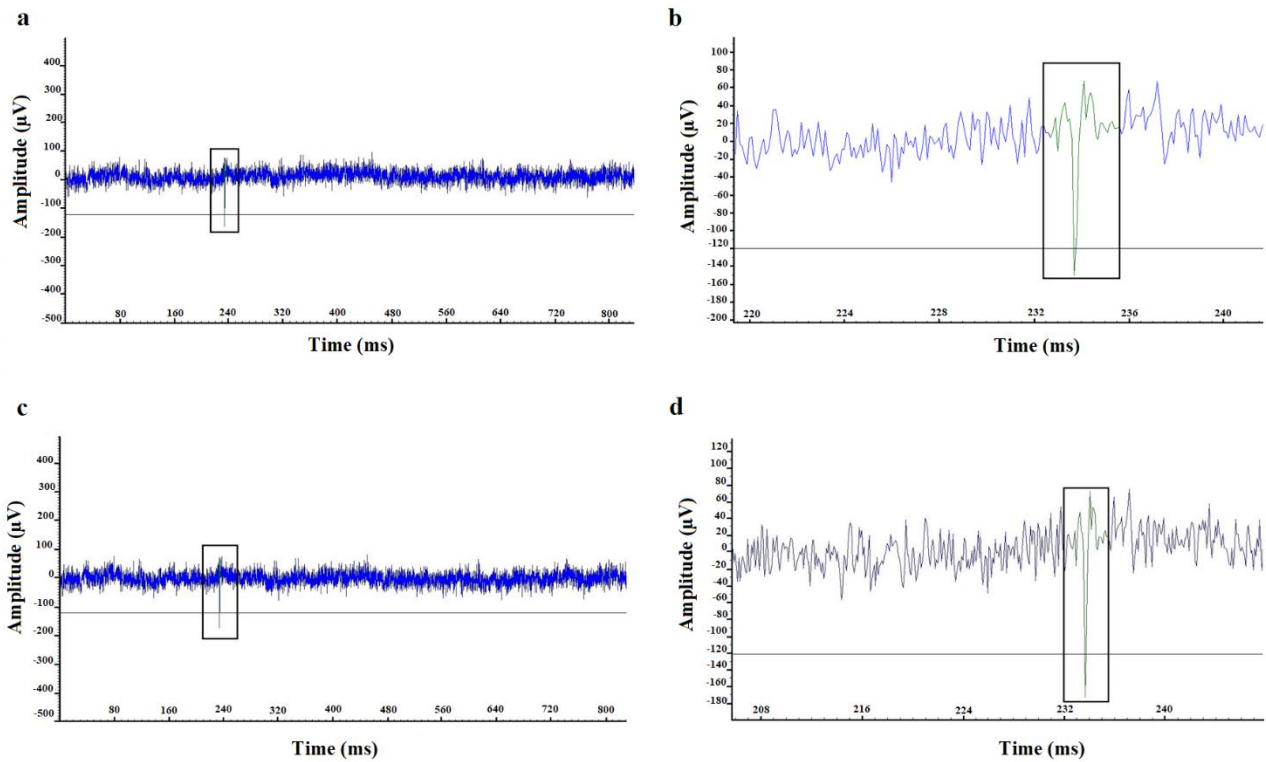
Figure 18. Spontaneous activity of the spiral ganglion neurons from a chip HM-F10-X3 (external reference electrode). a) Raw traces of the recorded spontaneous electrical activity in the primary spiral ganglion neurons at 9 DIV unveiling individual spike with an amplitude of 150µV; **b)** Profile of an individual spike with an amplitude of 150 µV corresponding to the black rectangle in a; **c)** Raw traces of the recorded spontaneous electrical activity in the primary spiral ganglion neurons at 9 DIV unveiling individual spike with an amplitude of 173 µV; **d)** Profile of an individual spike with an amplitude of 173 µV corresponding to black rectangle in c.
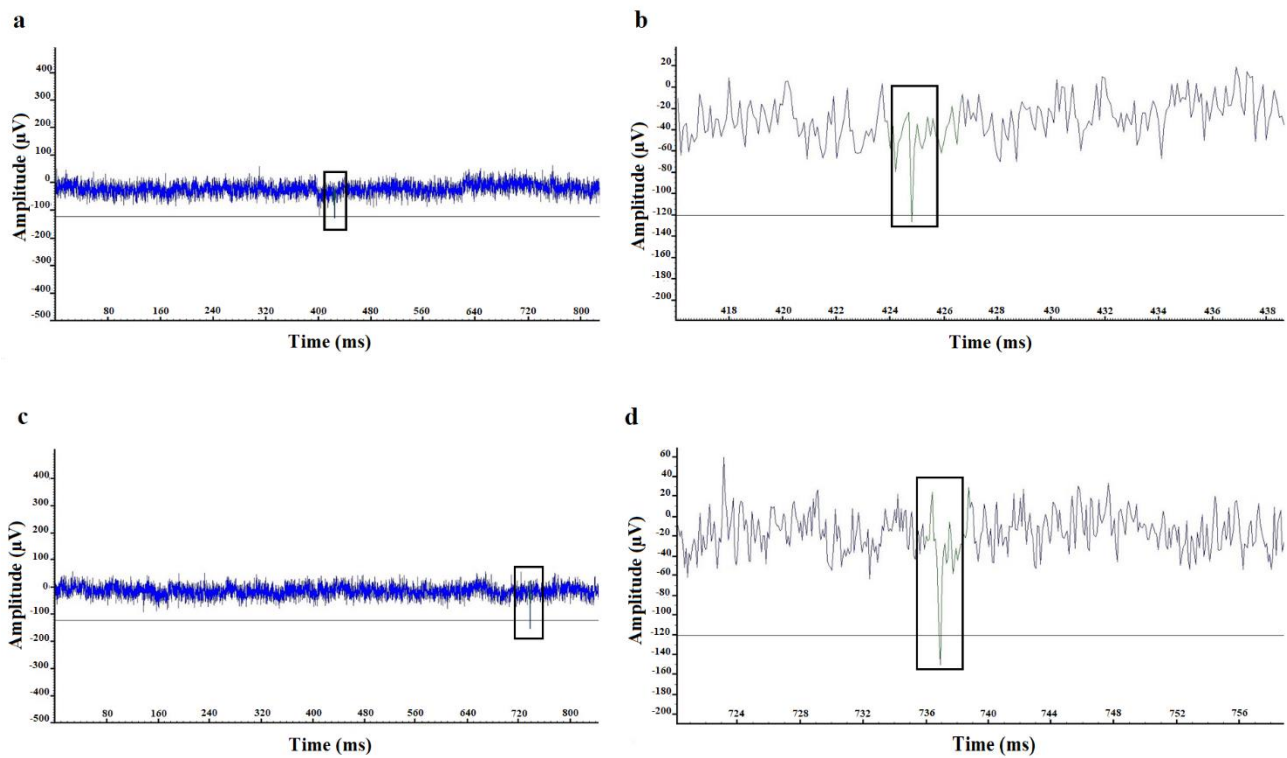
Figure 19. Neuronal voltages of the spiral ganglion neurons after stimulation from a chip HM-F10-X3 (stimulation after 60 s with current amplitude of 500nA, external reference electrode). a) Raw traces of the recorded electrical activity in the primary spiral ganglion neurons at 9 DIV after stimulation unveiling individual spike with an amplitude of 127 µV; **b)** Profile of an individual spike with an amplitude of 127 µV corresponding to the black rectangle in a; **c)** Raw traces of the recorded electrical activity in the primary spiral ganglion neurons at 9 DIV after stimulation unveiling individual spike with an amplitude of 150 µV; **d)** Profile of an individual spike with an amplitude 150 µV corresponding to the black rectangle in c.

To determine which neuron gives rise to a recorded signal, we stained neuronal cultures on the chip with neuronal marker Tuj and the electrode identified (Figure 20 and Figure 21).
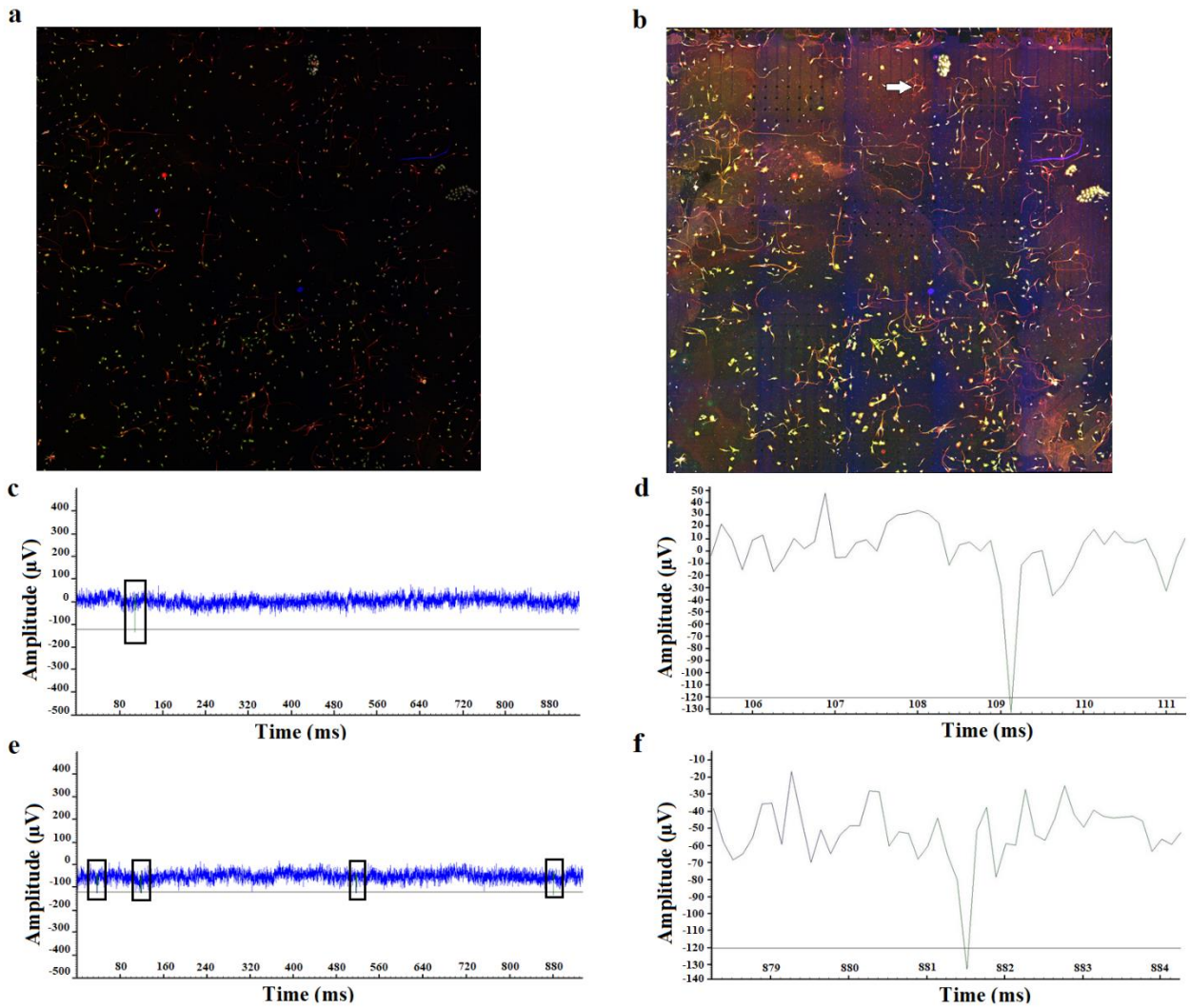
Figure 20. Fluorescent image, spontaneous activity, and neuronal voltages of the spiral ganglion neurons after stimulation from a chip HM-F8-X3. a) A fluorescent image of spiral ganglion neurons and glial cells from a whole chip at 6 DIV stained with a neuronal marker Tuj+ (red/magenta), a glial marker S-100 (green) and the nuclear marker DAPI (blue); **b)** A fluorescent image of spiral ganglion neurons and glial cells at 6 DIV from an entire chip with visible electrodes stained with a neuronal marker Tuj+ (red/magenta), a glial marker S-100 (green) and the nuclear marker DAPI (blue). A white arrow shows a 83rd electrode in the Electrode row 4 and a neurite from one of the neurons spanning this electrode; **c)** Raw traces of the recorded spontaneous electrical activity from 83rd electrode in the Electrode row 4 in the primary spiral ganglion neuron at 6 DIV from b unveiling individual spike with an amplitude of 133 µV; **d)** Profile of an individual spike with an amplitude of 133 µV corresponding to the black rectangle in c; **e)** Raw traces of the recorded electrical activity from 83rd electrode in the Electrode row 4 in the primary spiral ganglion neuron at 6 DIV from b after stimulation with current amplitude of 500 nA (external reference electrode) unveiling individual spikes with an amplitude of 125, 123, 123 and 134 µV; **f)** Profile of an individual spike with an amplitude of 134 µV corresponding to the fourth black rectangle in e.
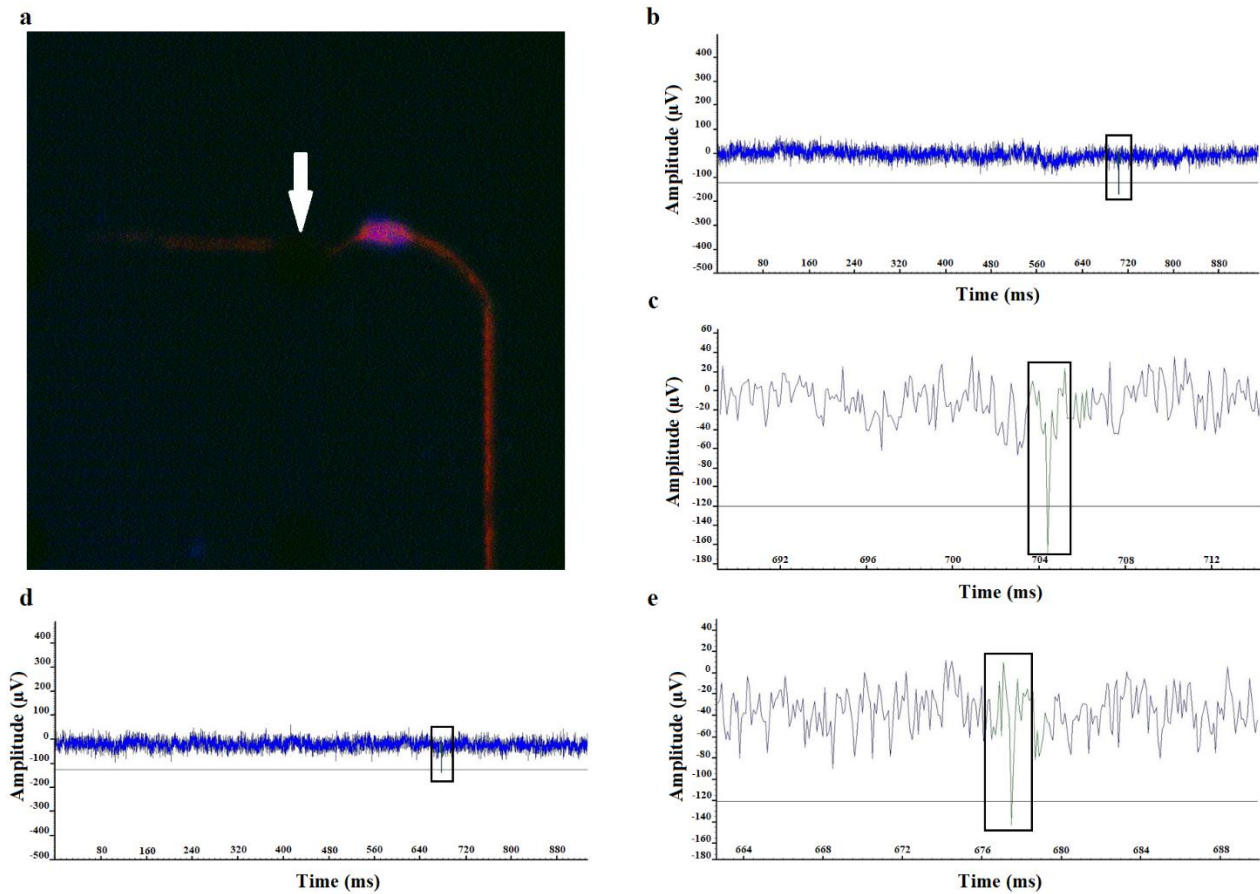
Figure 21. Fluorescent image, spontaneous activity, and neuronal voltages of the spiral ganglion neuron after stimulation from a chip HM-F10-X3. a) A fluorescent image of a spiral ganglion neuron at 7 DIV stained with a neuronal marker Tuj+ (red/magenta) and the nuclear marker DAPI (blue). A white arrow shows a 13th electrode in the Electrode row 1 and a neurite spanning this electrode; **b)** Raw traces of the recorded spontaneous electrical activity from 13th electrode in the Electrode row 1 in the primary spiral ganglion neuron at 7 DIV from a unveiling individual spike with an amplitude of 170 µV; **c)** Profile of an individual spike with an amplitude of 170 µV corresponding to the black rectangle in b; **d)** Raw traces of the recorded electrical activity from 13th electrode in the Electrode row 1 in the primary spiral ganglion neuron at 7 DIV from a after stimulation with current amplitude of 500 nA (external reference electrode) unveiling individual spike with an amplitude of 142 µV; **e)** Profile of an individual spike with an amplitude of 142 µV corresponding to the black rectangle in d.

In order to determine the neuronal origin of the detected spikes, spiral ganglion neurons were loaded with Fluo-4AM (Invitrogen, Belgium), a calcium indicator. Changes in intracellular calcium concentration were observed with an upright Examiner microscope (Carl Zeiss, Begium) equipped with a Hamamatsu-cooled CCD camera.
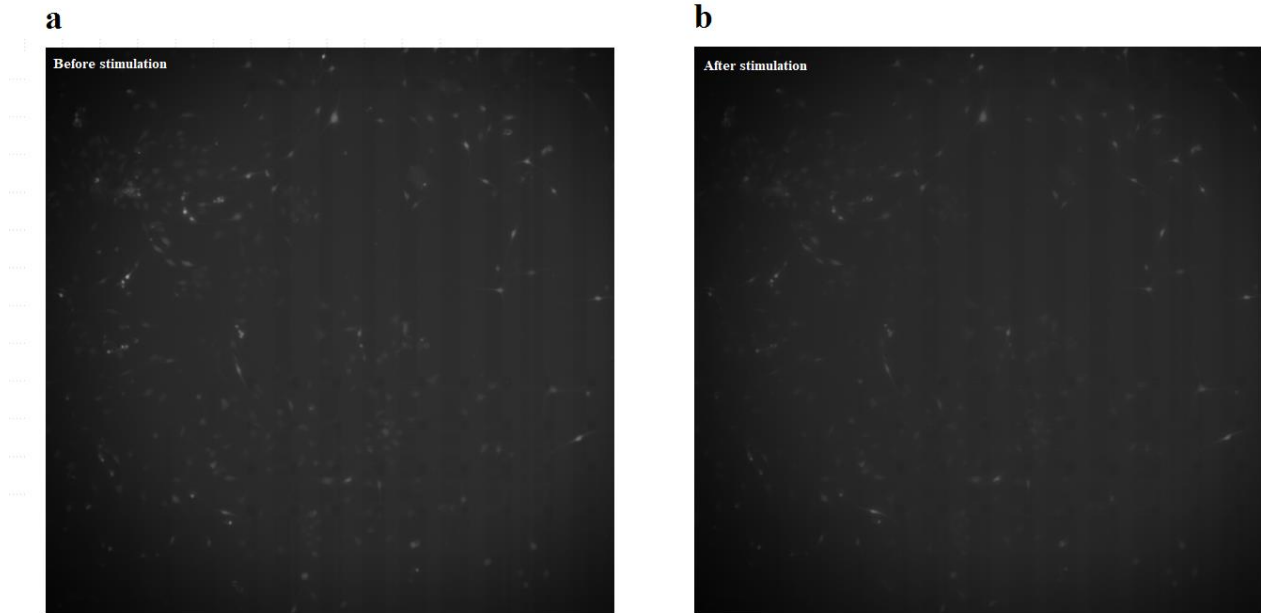
Figure 22. Changes of intracellular calcium in SGNs cultured on a chip HM-B10-X03. a) An image of changes in intracellular calcium in spiral ganglion neurons before stimulation on a chip HM-B10-X03-Electrode row 4. **b)** An image of changes in intracellular calcium after stimulation with a current amplitude of 500 nA on a chip HM-B10-X03-Electrode row 4.

5. DISCUSSION

5.1 Topographical cues of CMOS-MEA increase neuronal growth and survival rate

Our results demonstrate that micro-patterned and high-density CMOS-based electrode array represents an advantageous and favorable environment for *in vitro* SGN cultures by demonstrating more substantial cell presence of the SGN, faster neurite sprouting with strong bipolar morphological polarity, reduced neuronal-glial interactions, and the ability to stimulate the SGNs electrically. Micro-patterned surfaces of the CMOS substrates promoted neuronal growth more effectively than glass coverslips and even flat areas of the chip containing no protruding pillars (Figure 6c and Figure 7c). Findings were similar for neonatal and adult SGN cultures. Measurements of neurite lengths for neonatal and adult SGNs highlighted longer neurites, which also implies faster sprouting on CMOS chips than control (Figure 9a,b).

The study by Mattotti *et al* with dissociated neonatal SGN cultures on passive silicon micro-patterned surfaces, albeit with no active CMOS component, shows that neurons favor pillar spacing between 1.2 and 2.4 μm for improved growth and neurite elongation [36]. This study extended these findings by showing differences in neuronal distribution between neonatal and adult SGNs cultured on CMOS chips with different pillar widths and pillar spacing between 0.8 and 1.6 μm. To the best of our knowledge, this is the first study where SGNs demonstrate normal growth on non-coated micro-patterned CMOS surfaces as well (Figure 14), which can be useful in future clinical applications due to the degradation of the coating chemicals over time and safety issues. Cultures on non-coated glass coverslips are poorly attached, preventing neuronal growth on non-coated substrates. The flat surfaces of the non-coated chips showed poor neuronal growth because the neurons could not firmly attach without pillar support. These findings demonstrate that micro-patterned surfaces consisting of protruding pillars and embedded micro-electrodes provided with an advantageous environment for neuronal attachment and growth. Neonatal SGNs have shown preferential growth in areas with narrow and wide pillars, while adult SGNs prefer to grow on wide pillars. This outcome may be the consequence of either larger soma diameter or lower plating yield of adult SGNs, making a preference for wide pillars in adult SGNs. Repić *et al* study also found a similar observation for adult dorsal root ganglion neurons. Neonatal and adult SGNs on CMOS chips had the highest survival rates, whereas control glass coverslips induced weaker cell survival (Figure 6d and Figure 7d). The best survival rate was observed at 4 DIV, for both neonatal and adult SGNs, showing neuronal viability peaking around that time. We surmise that lower survival rates at 7 DIV are due to the proliferation of non-neuronal cells, such as glial cells, over time. This result is consistent with previous studies in which fibroblasts and glial cells proliferate, but neurons do not [72, 74, 75]. However, such a decrease was

significantly weaker on the micro-patterned surfaces of the CMOS chip. Compared with other studies reporting primary SGN cell cultures, our survival rates were comparable and even improved in some conditions. For instance, Jin *et al* [76] report a P5 SGN survival rate of 0.98% after 3 DIV, Vieira *et al* [65] describe the survival rate of adult SGNs from rats, mice or guinea pigs ranging between 1 and 6%, Mattotti *et al* [36] report a P5 SGN survival rate on MPS of 4.8% and Schwieger *et al* [12] describe P2-P4 SGN survival rate ranging from 3.57 to 40.69%, depending on the combination of different growth factors. Thus, the results in the present study confirm that micro-patterned CMOS substrates represent a more supportive and permissive environment for neuronal growth and survival compared to glass coverslips.

5.2 Micro-pillars of the CMOS-MEA with specific width and spacing induce neuronal orientation along preferred angles

Topographical cues strongly promote neuronal orientation and neurite guidance [33-37, 46, 77], as seen in SEM images (Figure 10) as well as polar plots of neural orientation showing neurite growth along 30°, 90°, and 150° radial angles, compared to the control where there was no preferred orientation of the neurites (Figure 10). SEM images highlight how SGNs develop their neurites in straight lines on top and between pillars (Figure 11). Only areas with pillars and micro-electrodes favor neurite alignment along preferred angles. These findings strongly suggest that pillar width and spacing significantly influenced SGN neurite orientation and alignment, which is crucial for structuring neurite connectivity. Pillars and micro-electrodes represent a strong and stable adhesion milieu where neurites are extended. It seems that the protruding shape and carefully crafted three-dimensional structure of pillars behave like geometrical constraints providing directional guidance. Closely spaced pillars and micro-electrodes stimulate neuronal growth by creating boosts at their contacts with neurons, compared to more separated pillars where signaling delay occurs. Other studies using silicon MPS [36, 37, 46] demonstrated that neurites were found to "search" for a new nearby permissive cue (pillar) and attach to areas with the largest pillar spacing, whereby this process elicits a structural change. Our SEM images also showed that the formation of nerve growth cones provided cells with a mechanical apparatus that guided neurite growth to mechanical, chemical, and electrical cues [78]. On micro-patterned surfaces of the CMOS chips, filopodia of the growth cone used pillars or micro-elecrodes as an anchoring point from where neuronal growth may occur.

5.3. CMOS-MEA substrates promote bipolar and multipolar morphology of spiral ganglion neurons cultured in vitro

The presence of micro-pillars and micro-electrodes on CMOS chips also strongly influenced SGN morphology. The number of neurons with bipolar and multipolar morphologies grown on CMOS substrates was stable over time, while the number of neurons with monopolar and other morphologies was significantly reduced compared to the control group. Mattotti *et al* reported that neonatal SGNs developed more monopolar and bipolar morphologies when they were cultured on MPSs. At the same time, there was a reduction in the number of neurons with multipolar morphologies and concluded that MPSs might be more beneficial to induce neuronal morphologies more similar to *in vivo* conditions [36]. Our study with neonatal and adult SGNs cultured on CMOS chips demonstrated that CMOS substrates encouraged neurons to develop more bipolar and multipolar morphologies. *In vitro* neurite-free, mono-, bi- and multi-polar morphologies were also observed in other studies [12, 17, 65, 66, 77]. Different sprouting behaviors can be related to neuronal polarization and neurite pathfinding [35]. The appearance of SGNs *in vitro* may vary between studies, depending on the species of origin, the age of the animals, and the cell culture protocol [17, 36, 79]. Khalifa *et al* reported a drastic increase in the number of multipolar neurons from 5% on non-structured surfaces to 86–87% on surfaces with alternating lines [80]. They stated that controlled sprouting and branching can be an essential process in the sense that additional neurites contribute to augmenting the chances that neurites reach their targets [80]. We hypothesize that the micro-topography of CMOS chips probably utilizes similar stimulation mechanisms that could be integrated synergistically with biochemical support to design optimal electrode arrays. The comparison of our results with the results of other studies is difficult because of the different materials, sizes, shapes, and uniformities of the CMOS chips, as well as different techniques used for the analysis of the alignment and neuronal behavior and measurements.

5.4 Topographical structures of CMOS-MEA discourage neuronal contact with glial cells and promote neuronal interaction with pillars and grooves

In vitro cultures of SGNs also comprise a significant number of non-neuronal cells, primarily glial cells, where the ratio to neurons can vary, for example, from 1:1 to 20:1 [6, 65]. However, our study suggests different ratios of glial cells/neurons. The ratio of glial cells/neurons of neonatal SGNs increased over time, from 2.3 ± 0.6 (4 DIV) to 5.1 ± 1.2 (7 DIV) on CMOS chips and from 3.2 ± 0.9 (4 DIV) to 8.6 ± 3.7 (7 DIV) on control glass coverslips, due to glial cell proliferation. On the other hand, the opposite effect was found for adult neurons since the ratio of glial cells/neurons decreased over time, from 2.6 ± 1.0 to 2.1 ± 0.7 (4 DIV) on CMOS chips and from 3.6 ± 1.3 to 2.9 ± 1.1 (7

DIV) on control glass coverslips. This outcome might be related to the age of animals and animal species since other studies [65, 66, 74, 75, 81] reported that the density of non-neuronal cells decreased with increasing age of the animal, which can explain why dissociated SGN cultures of mature animals could be maintained for several weeks. The proliferation of glial cells was slower on the micro-patterned surfaces of the CMOS chip in both neonatal and adult SGN cultures, shown by lower ratios of glial cells/neurons, which increased the survival rate of neurons in these areas. Schwann and satellite cells are the most commonly SGN-associated cells in the spiral ganglion or spiral lamina, and they are immune-reactive for the marker S100 [72, 73]. These types of glial cells play an essential role in neuronal growth, survival, regeneration, and axonal guidance *in vivo* and *in vitro* [36, 44, 72, 80]. It has been shown that SGNs in culture prefer to grow in proximity to glial cells due to the adhesive molecular patterns, like Laminin-1, that these cells secrete [36, 44, 72]. Our data show that neurites of the neonatal and adult SGNs on CMOS substrates were encouraged to grow more in direct contact with micro-pillars and micro-electrodes rather than to seek interaction with glial cells that were present in their surroundings. In fact, SGNs (Figure 9c, d) intertwined their neurites, exchanging information from the environment instead of being in contact with glial cells. Neonatal SGNs have shown a tendency towards highly patterned neuronal networks promoting connections between neurites while discouraging contacts with glial cells. Previous studies by several groups [35, 36, 41, 44, 77, 82, 83] demonstrated cytoskeletal alterations and upstream signaling related to neurons interacting with pillars and grooves, indicating consistency with our findings, suggesting that topographic cues presented with micro-pillars on CMOS chips support direct neurite guidance without the mediating action of glial cells. These factors, taken together, create a favorable environment for neuronal growth and neurite sprouting.

5.5 CMOS-MEA substrates enable the presence of Type I and Type II spiral ganglion neurons

The mature mammalian cochlea exhibits segregated innervation of its two populations of sensory hair cells, inner hair cells (IHC) and outer hair cells (OHC), by the SGNs [16, 78]. Type I SGNs comprise 90 to 95% of the SGN population and extend single, unbranched, myelinated neurites to innervate a single inner hair cell (IHC) [16, 78]. The IHCs with Type I SGN innervation are responsible for the signal transduction of sound stimuli to be delivered upstream along the auditory pathway [16, 78]. The remaining 5 to 10% of SGN are Type II neurons with thin, unmyelinated fibers innervating numerous outer hair cells (OHCs) [16, 78]. Adult SGNs cultured on glass coverslips and CMOS chips were stained with Tuj and peripherin to distinguish between Type I and Type II SGNs. Peripherin positive (appeared in green) [16] neurons were identified as Type II SGNs (Figure 12). Only SGNs isolated from adult guinea pigs were stained with peripherin antibodies because neonatal Type II

SGNs occurred between 6 to 8 DIV. At that time, it was impossible to distinguish between two neuronal types as observed morphological differences develop only later [17, 84]. Consequently, rat pups are an inappropriate model for investigating the appearance of Type II SGNs. The presence of Type II SGNs on CMOS chips indicates the ability of the micro-structured surfaces to promote the natural appearances of both types of SGNs that are important for natural cochlear innervation.

5.6 Bipolar spiral ganglion neurons have two asymmetrical processes

Based on the position of the soma relative to the central process (usually referred to as the axon) and the peripheral process (usually referred to as the dendrite), neurite width asymmetry between these two processes in bipolar neurons can be observed in Type I SGN [16]. This asymmetry is shown in SEM images (Figure 13) and was statistically quantified.

5.7 Position of neuronal soma and neurites on microelectrodes influences electrophysiological recordings

Spiral ganglion neurons have an unusual morphological configuration in which electrogenic soma reside directly in the signal transduction pathway, representing an internodal axonal structure that serves for transmitting, integrating, and conducting signals [1]. The position of the micro-electrodes within the CMOS chip is undoubtedly an essential aspect of electrophysiological recordings. The electrical activity of the SGNs can presumably be recorded if an electrogenic soma is positioned directly on the top of a micro-electrode or the neurite spans the micro-electrode, ensuring neuron-electrode proximity. In this study, considering the extremely demanding and sensitive *in vitro* conditions for peripheral sensory neurons, we showed that there is a sufficient number of SGNs either with soma placement directly on the top of a micro-electrode or a neurite spanning a micro-electrode, or both, which represent realistic requirements for electrophysiological applications. These findings were confirmed with live calcium imaging experiments of SGN cultures, which were electrically stimulated with the CMOS electrode array. We observed that neurons with either soma positioned directly on the top of a micro-electrode or the neurite contacting the micro-electrode had shown a substantial increase in the $[Ca^{2+}]_i$ after being stimulated with biphasic pulse trains. The fast increase in the $[Ca^{2+}]_i$ could be caused by two mechanisms: opening of voltage-gated Ca^{2+} channels causing an influx of extracellular Ca^{2+} during stimulation and formation of pores along the membrane, allowing extracellular Ca^{2+} to flow inside the cell.

5.8 Advantages and disadvantages of patch-clamp technique as observed from previous studies

Up to now, electrophysiological properties of the spiral ganglion neurons have been performed using patch clamp techniques. This technique enables intracellular recordings of action potentials and detailed analysis of intracellular ionic currents from single neurons. Heterogeneity in firing properties and voltage-dependent ionic currents of SG neurons were previously described depending on the apical or basal location of the neurons [11, 85, 86, 87], as well as dependent on different neurotrophins, namely BDNF and NT3, exogenously provided to the culture [11, 88, 89]. However, patch clamp is an invasive method, including rupturing cell membrane, which is reflected in the inherent short cell viability time [50, 90]. The technique is naturally limited in the proximity and number of patch clamp electrodes that can be used at any one time and in the number of cells or the number of points on a single cell that can be simultaneously measured [50, 90]. The settings of each recording electrode vary by laboratory depending on the puller and type of glass used. The inner diameter and the resistance of the recording pipette depend on the temperature provided by each stage of the two-stage pull program [91]. All these obstacles make the patch clamp technique more challenging to perform. All patch-clamp recordings from different groups were made at room temperature (19-22°C) [85, 86, 87, 88, 89, 91]. Heterogeneity in both threshold and timing-related features was noted in previous works in which dissociated cultures of apical and basal thirds of the ganglion were used [92]. Liu *et al* showed that the heterogeneous properties of SGNs are distributed locally [86]. Timing-related features, such as onset kinetics, latency, and accommodation, were graded from the high-frequency basal neurons to the low-frequency apical ones, corresponding to the tonotopic map [86]. Threshold sensitivity, however, was highest in the middle region of the cochlea in a pattern that appears to be coincident with the best-frequency area [86]. Studies have shown that voltage-gated ion channel α-subunit distributions in postnatal and adult animals, and hence spiral ganglion neurons electrophysiology is potently regulated by the brain-derived neurotrophic factor (BDNF) and neurotrophin-3 (NT-3) [92]. Neurons supplemented with low concentrations of BDNF uniformly showed rapid accommodation, abbreviated latency, and rapid onset tau, along with enhanced ion channel α-subunits associated with the rapid basal neurons (Kv3.1, Kv1.1, Kv1.2, BK). In contrast, neurons supplemented with low concentrations of NT-3 showed a more heterogeneous profile that included a more significant proportion of cells with slow accommodation, prolonged latencies, and slow onset tau, along with enhanced Kv4.2 α-subunits [92].

5.9 CMOS-MEA is a favorable tool for recording spontaneous neuronal activity and electrically stimulating dissociated spiral ganglion neurons

In this study, an *in vitro* bioassay, based on a non-invasive electrophysiological characterization of SGNs on CMOS-like electrode array, that can be used to study activity profiles of SGNs by analyzing spontaneous activity or responses to extracellular stimulation of many dissociated neurons simultaneously, is presented. Since SGNs do not form a neuronal network among themselves but act as bipolar neurons connecting sensory hair cells to the cochlear nucleus, CMOS-like electrode arary is used in this setting for parallel simultaneous measurements of unconnected neurons and thus for characterization of the direct group response to stimulation. To the best of our knowledge, this study shows for the first time that stimulation and recording of auditory neuronal activity from dissociated SGNs cultures using CMOS-like electrode array is feasible. We performed all electrophysiological experiments at 37°, similar to the body temperature of homoeothermic organisms like humans, rats, mice, and other animals. Spontaneous activity detection started from day six onwards, being the earliest time point assessed, and an increase was observed with prolonged culture time, which is in agreement with the increase in neuron coverage of the electrode area. Older cultures appear to provide more reliable results. Besides recording spontaneous activity (Figure 17a, b, Figure 18), the MEA setup presented in this study also allowed us to comparatively assess electrical stimulation parameters for dissociated SGNs cultures (Figure 17c,d, Figure 19). A biphasic (positive first) stimulus with a total duration of 60 μs and an amplitude of 500 nA or 800 nA was used for stimulation. When stimulating the culture, particular caution should be used in selecting the stimulus as large amplitudes (>3V), and durations may cause damage to the culture [93]. External Pt foil reference electrode or internal Pt foil reference electrode was used, and no differences in responses between the two reference electrodes were not observed. Immunostaining of SGNs cultures on MEA for the neuronal marker Tuj revealed both somata as well as processes of neurons on the electrode surface (Figure 20a, b, Figure 21a), similar to results showing that the position of neuronal soma and neurites affects recordings of electrical activity on MEA. The average maximum spike amplitude was 135.4 ± 15.2 μV for recorded spontaneous activity and 130 ± 10 μV for recorded neural activity after stimulation. An intracellular concentration of Ca^{2+} in SGNs before and after electrical stimulation was observed to confirm the neuronal origin of the detected action potentials. Figure 22 shows changes in Ca^{2+} concentration before stimulation, which reflects spontaneous neuronal activity, and after stimulation, which is due to neuronal responses to stimulation. Calcium imaging was also performed on SGNs cultured on glass coverslips, and changes in intracellular Ca^{2+} were also observed, confirming spontaneous activity in SGNs. One of the first studies that utilized MEAs for assessing electrophysiological characteristics of SGNs *in vitro* was from Hahnewald *et al* [11, 93]. They used

SGN explants and a MEA containing 68 platinum electrodes with a dimension of 40x40 μm and an inter-electrode distance of 200 μm and showed that the stimulation and recording of auditory neuronal activity from SGN explants using MEA is possible. They have been assessing the distance-dependent response of the auditory neurons to an external stimulating electrode and confirmed that the efficiency of SGN stimulation is increased by decreasing the distance between the stimulating electrode and the auditory neuron culture. In this study, CMOS chips with a much higher number of integrated microelectrodes (Neuray II chips) and CMOS-like chips (HearMe chips) with integrated microelectrodes with a diameter of 20 μm, an inter-electrode distance of 100 μm and pillars with a pillar width of 1, 1.8, 2.8 and 4 μm and pillar spacing of 2 μm covering the whole surface of the chip that both enable successful electrical stimulation of dissociated SGN cultures, are presented. Previous studies have shown that the pillars of the electrode array maintain a stable environment for SGNs cultured *in vitro* and can guide neurites towards electrodes [36, 46, 77], while microelectrodes enable electrophysiological stimulation of each neuron. A smaller inter-electrode distance of the electrode array encourages closer contact between auditory neurons and electrodes, which can result in lower stimulation thresholds [77]. The future optimal design of the CMOS MEA chip will include a chip area covered with micro-pillars, without a flat surface and a high number of integrated microelectrodes for stimulation. A study from Miccoli *et al* [94] reported the successful cultivation of primary rat hippocampal neurons on a multimodal CMOS MEA chip *in vitro* and their electrophysiological activity over time. They showed a mean spike amplitude of 144.8 ± 84.6 μV and that the signal amplitude can be significantly reduced due to spatial-averaging effects across the recording area of the electrodes [94]. They detected a higher maximum spike amplitude by smaller electrodes than larger ones. [94]. The rate of responses to stimulation mainly depends on the neuronal density in the culture, the contacts between neurons and electrodes, the diameter of neuronal soma or neurite, and electrode impedance. Neuronal density, soma, and neurite size are highly sensitive to SGN isolation and culture conditions, so careful dissection of the spiral ganglion and further handling of the primary cultures require particular caution. Pillars of the electrode array enable firm contact of the neuronal neurites with the electrodes and enhance neuronal growth. The electrodes' size and surface mainly determine the electrodes' impedance. Materials such as black platinum or titanium nitride form high-surface area coatings with low electrode impedance, which improves electric noise performance [50]. Overall, these findings suggest micro-patterned and high-density complementary metal–oxide–semiconductor electrode array as a promising model of a neuro-electronic interface that supports neuronal growth, alignment, and orientation of *in vitro* cultured spiral ganglion neurons and which can electrically stimulate neurons. We assume that electrical cues of micro-patterned and high-density CMOS electrode arrays would enable growth stimulation of regenerating neurites of spiral

ganglion neurons, attracting them toward electrodes. The model presented in this study is a very useful *in vitro* tool to investigate strategies to improve the efficacy of stimulation of auditory neurons and further optimize CI technology. Future *in vitro* and *in vivo* studies will be necessary to elucidate the electrophysiological properties of auditory neurons interfaced with types of micro-patterned and high-density CMOS electrode arrays.

6. CONCLUSION

The main conclusions after the completed experimental research are:

- Micro-patterned and high-density complementary metal–oxide–semiconductor electrode array represents a promising model for a neuro-electronic interface that supports neuronal growth, alignment, and orientation of *in vitro* cultured spiral ganglion neurons.

- Electrophysiological response profiles of auditory neurons can be reliably obtained with such electrode arrays.

- CMOS chips and CMOS-like chips can be used for recording spontaneous activity and neuronal activity after electrical stimulation of dissociated spiral ganglion neurons cultured *in vitro.*

- Compared to the patch clamp technique, which is an invasive method where cell viability and the overall number of cells that can be simultaneously recorded are limited with time, the significant advantages of using CMOS technology include connectivity with on-chip multiplexing architectures that can address large numbers of electrodes, signal quality with conditioning signals right at the electrode using dedicated circuitry units (filters, amplifiers) and finally ease of handling and use with many functions that can be programmed or automated via user-friendly software and digital interfaces that directly address digital registers and logic or memory units on the chip side.

- The model presented in this study represents a novel *in vitro* tool to investigate strategies for simultaneous electrical stimulation and recording of auditory neurons to optimize CI technology.

7. LITERATURE

1. Dabdoub A, Fritzsch B, Popper AN, Fay RR. The primary auditory neurons of the mammalian cochlea. 2015, New York: Springer.

2. Kaiser, O. G. et. al. TGF-beta superfamily member activin A acts with BDNF and erythropoietin to improve survival of spiral ganglion neurons *in vitro*. . 2013, 75: 416-425.

3. Euteneuer, S. et al. Glial cell line-derived neurotrophic factor (GDNF) induces neuritogenesis in the cochlear spiral ganglion via neural cell adhesion molecule (NCAM*). Mol Cell Neurosci.* 2013, 54: 30-43.

4. Lu CC, Appler JM, Houseman EA, Goodrich LV. Developmental profiling of spiral ganglion neurons reveals insights into auditory circuit assembly. *J Neurosci*. 2011, 31 (30): 10903-10918.

5. Lefebvre PP, Malgrange B, Lallemend F, Staecker H, Moonen G, Van de Water TR. Mechanisms of cell death in the injured auditory system: otoprotective strategies. Audiol Neuro Otol. 2002, 7: 165–170.

6. Rask-Andersen H, Liu W, Erixon E, Kinnefors A, Pfaller K, Schrott-Fischer A, et al. Human cochlea: anatomical characteristics and their relevance for cochlear implantation. *Anat Rec (Hoboken.)* 2012, 295: 1791-1811.

7. Wilson BS, Dorman MF. Cochlear implants: a remarkable past and a brilliant future. *Hearing Research.* 2008, 242: 3-21.

8. Zeng FG, Rebscher S, Harrison W, Sun X, Feng H. Cochlear implants: system design, integration and evaluation. *IEEE Rev Biomed Eng.* 2008, 1: 115-142.

9. Blamey P, Barry J, Bow C, Sarant J, Paatsch L, Wales R. The development of speech production following cochlear implantation. *Clinical Linguistics and Phonetics*. 2001, 15: 363–82.

10. Shepherd RK, Hardie NA. Deafness-induced changes in the auditory pathway: implications for cochlear implants. *Audiol Neurootol.* 2001, 6: 305-318.

11. Hahnewald S, Tscherter A, Marconi E, Streit J, Widmer HR, Garnham C, et al. Response profiles of murine spiral ganglion neurons on multi-electrode arrays. *Journal of Neural Engineering.* 2016, 13: 1-14.

12. Schwieger J, Warnecke A, Lenarz T, Esser KH, Scheper V. Neuronal Survival, Morphology and Outgrowth of Spiral Ganglion Neurons Using a Defined Growth Factor Combination. *PLoS One.* 2015, 10: e0133680.

13. Shibata SB, Budenz CL, Bowling SA, Pfingst BE, Raphael Y. Nerve maintenance and regeneration in the damaged cochlea. *Hearing Research.* 2011, 281: 56-64.

14. Kollmeier B. Anatomy, Physiology and Function of the Auditory System. In: Havelock D., Kuwano S., Vorländer M. (eds) Handbook of Signal Processing in Acoustics. 2008, Springer, New York, NY, pp 147-158.

15. Coate TM, Kelley MW. Making connections in the inner ear: recent insights into the development of spiral ganglion neurons and their connectivity with sensory hair cells. *Semin Cell Dev Biol.* 2013, 24: 460-469.

16. Nayagam BA, Muniak MA & Ryugo D.K. The spiral ganglion: connecting the peripheral and central auditory systems. *Hearing Research.* 2011, 278: 2-20.

17. Rusznák Z & Szucs G. Spiral ganglion neurones: an overview of morphology, firing behaviour, ionic channels and function. *Pflugers Arch.* 2009, 457: 1303-1325.

18. Rosenbluth J. The fine structure of acoustic ganglia in the rat. *Journal of Cell Biology.* 1962, 12: 329–359.

19. Nadol JB, Jr. Burgess BJ, & Reisser C. Morphometric analysis of normal human spiral ganglion cells. *Annals of Otology, Rhinology, and Laryngology.* 1990, 99: 340–348.

20. Hossain WA, Antic SD, Yang Y, Rasband MN, & Morest DK. Where is the spike generator of the cochlear nerve? Voltage-gated sodium channels in the mouse cochlea. *The Journal of Neuroscience.* 2005, 25 (29): 6857–6868.

21. Robertson D. Possible relation between structure and spike shapes of neurones in guinea pig cochlear ganglion. *Brain Research*. 1976, 109 (3): 487–496.

22. Chen WC, Xue HZ, Hsu YL, Liu Q, Patel S, & Davis RL. Complex distribution patterns of voltage-gated calcium channel alpha-subunits in the spiral ganglion. *Hearing Research*. 2011, 278 (1–2): 52–68.

23. Bailey EM & Green SH. Postnatal expression of neurotrophic factors accessible to spiral ganglion neurons in the auditory system of adult hearing and deafened rats. *The Journal of Neuroscience*. 2014, 34 (39): 13110-13126.

24. Fritzsch B, Tessarollo L, Coppola E, Reichardt LF. Neurotrophins in the ear: their roles in sensory neuron survival and fiber guidance. *Prog Brain Res*. 2004, 146: 265–278.

25. Sugawara M, Murtie JC, Stankovic KM, Liberman MC, Corfas G. Dynamic patterns of neurotrophin 3 expression in the postnatal mouse inner ear. *J Comp Neurol*. 2007, 501: 30 –37.

26. Malgrange B, Lefebvre P, Van de Water TR, Staecker H, Moonen G. Effects of neurotrophins on early auditory neurones in cell culture. *Neuroreport*. 1996, 7: 913–917.

27. Hegarty JL, Kay AR, Green SH. Trophic support of cultured spiral ganglion neurons by depolarization exceeds and is additive with that by neurotrophins or cyclic AMP, and requires elevation of [Ca 2_]i within a set range. *J Neurosci*. 1997, 17: 1959 –1970.

28. Ernfors P, Duan ML, ElShamy WM, Canlon B. Protection of auditory neurons from aminoglycoside toxicity by neurotrophin-3. *Nat. Med.* 1996, 2 (4): 463-467.

29. Staecker H, Kopke R, Malgrange B, Lefebvre P, Van de Water TR. NT-3 and/or BDNF therapy prevents loss of auditory neurons following loss of hair cells. *Neuroreport*. 1996, 7: 889–894.

30. Ylikoski J, Pirvola U, Moshnyakov M, Palgi J, Aruma¨e U, Saarma M. Expression patterns of neurotrophin and their receptor mRNAs in the rat inner ear. *Hear Res*. 1993, 65: 69 –78.

31. Ylikoski J, Pirvola U, Virkkala J, Suvanto P, Liang XQ, Magal E, Altschuler R, Miller JM, Saarma M. Guinea pig auditory neurons are protected by glial cell line-derived growth factor from degeneration after noise trauma. *Hear Res*. 1998, 124: 17–26.

32. Warnecke A, Scheper V, Buhr I, Wenzel GI, Wissel K, Paasche G, Berkingali N, Jørgensen JR, Lenarz T, Sto¨ver T. Artemin improves survival of spiral ganglion neurons *in vivo* and *in vitro*. *Neuroreport*. 2010, 21 (7): 517-521.

33. Fozdar DY, Lee JY, Schmidt CE, Chen S. Hippocampal neurons respond uniquely to topographies of various sizes and shapes. Biofabrication. 2010, 2: 035005.

34. Hoffman-Kim D, Mitchel JA, Bellamkonda RV. Topography, cell response, and nerve regeneration. *Annu Rev Biomed Eng.* 2010, 12: 203-231.

35. Micholt L, Gärtner A, Prodanov D, Braeken D, Dotti CG, Bartic C. Substrate topography determines neuronal polarization and growth in vitro. *PLoS One.* 2013, 8: e66170.

36. Mattotti M, Micholt L, Braeken D, Kovačić D. Characterization of spiral ganglion neurons cultured on silicon micro-pillar substrates for new auditory neuro-electronic interfaces. *J Neural Eng*. 2015, 12: 026001.

37. Repić T, Madirazza K, Bektur E, Sapunar D. Characterization of dorsal root ganglion neurons cultured on silicon micro-pillar substrates. *Sci Rep.* 2016, 6: 39560.

38. Rajnicek A, Britland S, McCaig C. Contact guidance of CNS neurites on grooved quartz: influence of groove dimensions, neuronal age and cell type. *J Cell Sci.* 1997, 110: 2905-2913.

39. Rajnicek A, McCaig C. Guidance of CNS growth cones by substratum grooves and ridges: effects of inhibitors of the cytoskeleton, calcium channels and signal transduction pathways. *J Cell Sci*. 1997, 110: 2915-2924.

40. Ferrari A, Faraci P, Cecchini M, Beltram F. The effect of alternative neuronal differentiation pathways on PC12 cell adhesion and neurite alignment to nanogratings. *Biomaterials*. 2010, 31: 2565-2573.

41. Ferrari A, Cecchini M, Serresi M, Faraci P, Pisignano D, Beltram F. Neuronal polarity selection by topography-induced focal adhesion control. *Biomaterials*. 2010, 31: 4682-4694.

42. Tuft BW, Li S, Xu L, Clarke JC, White SP, Guymon BA, *et al.* Photopolymerized microfeatures for directed spiral ganglion neurite and Schwann cell growth. *Biomaterials*. 2013, 34 :42-54.

43. Tuft BW, Xu L, White SP, Seline AE, Erwood AM, Hansen MR, *et al.* Neural pathfinding on uni- and multidirectional photopolymerized micropatterns. *ACS Appl Mater Interfaces*. 2014, 6: 11265-11276.

44. Clarke J C, Tuft BW, Clinger JD, Levine R, Figueroa LS, Guymon CA, *et al.* Micropatterned methacrylate polymers direct spiral ganglion neurite and Schwann cell growth. *Hear Res*. 2011, 278: 96-105.

45. Xu L, Seline AE, Leigh B, Ramirez M, Guymon CA, Hansen MR. Photopolymerized microfeatures guide adult spiral ganglion and dorsal root ganglion neurite growth. *Otol Neurotol.* 2017, 39: 119-126.

46. Radotić V, Bedalov A, Drviš P, Braeken D, Kovačić D. Guided growth with aligned neurites in adult spiral ganglion neurons cultured *in vitro* on silicon micro-pillar substrates. *J Neural Eng.* 2019, 16: 066037.

47. Braeken D, Huys R, Jans D, Loo J, Severi S, Vleugels F, *et al*. Local electrical stimulation of single adherent cells using three-dimensional electrode arrays with small interelectrode distances. *Conf Proc IEEE Eng Med Biol Soc*. 2009, 2009: 2756-2759.

48. Braeken D, Huys R, Loo J, Bartic C, Borghs G, Callewaert G, *et al*. Localized electrical stimulation of in vitro neurons using an array of sub-cellular sized electrodes. *Biosens Bioelectron*. 2010, 26: 1474-1477.

49. Braeken D, Jans D, Huys R, Stassen A, Collaert N, Hoffman L, *et al*. Open-cell recording of action potentials using active electrode arrays. *Lab on a Chip*. 2012, 12, 4397-4402.

50. Hierlemann A, Frey U, Hafizovic S & Heer F. Growing cells atop microelectronic chips: Interfacing electrogenic cells in vitro with CMOS-based microelectrode array. *Proceedings of the IEEE*. 2011, 99, 252-284.

51. Huys R, Braeken D, Jans D, Stassen A, Collaert N, Wouters J, *et al*. Single cell recording and stimulation with a 16k micro-nail electrode array integrated on a 0.18 μm CMOS chip. *Lab on a chip*. 2012, 12, 1274-1280.

52. Leake PA, Hradek GT & Snyder RL. Chronic electrical stimulation by a cochlear implant promotes survival of spiral ganglion neurons after neonatal deafness. *J. Comp. Neurol.* 1999, 412: 543-562.

53. Leake PA, Stakhovskaya O, Hetherington A, Rebscher SJ. Bonham, B. Effects of brain-derived neurotrophic factor (BDNF) and electrical stimulation on survival and function of cochlear spiral ganglion neurons in deafened developing cats. *J. Assoc. Res. Otolaryngol*. 2013, 14: 187-211.

54. Maher MP, Pine J, Wright J & Tai YC. The neurochip: A new multielectrode device for stimulating and recording from cultured neurons.. *J. Neurosci Methods*. 1999, 87: 45–56.

55. Martinoia S, Massobrio P, Bove M, Massobrio G. BCultured neurons coupled to microelectrode arrays: Circuit models, simulations and experimental data. *IEEE Trans. Biomed. Eng*. 2004 51 (5): 859–864.

56. Heuschkel MO, Fejtl M, Raggenbass M, Bertrand D, Renaud P. A three-dimensional multi-electrode array for multi-site stimulation and recording in acute brain slices. *J. Neurosci. Methods*. 2002, 114 (2): 135-148.

57. Wallrapp F & Fromherz P. BTiO2 and HfO2 in electrolyte-oxide-silicon configuration for applicationsa in bioelectronics. *J. Appl. Phys*. 2006, 99: 114103.

58. Schoen I & Fromherz P. The mechanism of extracellular stimulation of nerve cells on an electrolyte-oxide-semiconductor capacitor. *Biophys. J*. 2007, 92: 1096–1111.

59. Greve F, Frerker S, Greet Bittermann A, Burkhardt C, Hierlemann A, Hall H. Molecular design and characterization of the neuron-microelectrode array interface. *Biomaterials*. 2007, 28: 5246–5258.

60. Soussou WV, Yoon GJ, Brinton RD, Berger TW. Neuronal network morphology and electrophysiology of hippocampal neurons cultured on surface-treated multielectrode arrays,[IEEE Trans. Biomed. Eng. 2007, 54 (7): 1309–1320.

61. Emmenegger V, Obien MEJ, Franke F, Hierlemann A. Technologies to study action potential propagation with a focus on HD-MEAs. *Front. Cell. Neurosci.* 2019, 13: 159.

62. Rochefort NL, Jia H, Konnerth A. Calcium imaging in the living brain: Prospects for molecular medicine. *Trends Mol Med*. 2008, 14 (9): 389-399.

63. Miyazaki K, Ross WN. Simultaneous sodium and calcium imaging from dendrites and axons. *eNeuro*. 2015, 2 (5): 1-10.

64. Russel JT. Imaging calcium signals *in vivo*: a powerful tool in physiology and pharmacology. *Br J Pharmacology*. 2011, 163 (8): 1605-1625.

65. Vieira M, Christensen BL, Wheeler BS, Feng AS & Kollmar R. Survival and stimulation of neurite outgrowth in a serum-free culture of spiral ganglion neurons from adult mice. *Hearing Research.* 2007, 230: 17-23.

66. Whitlon DS, Ketels KV, Coulson MT, Williams T, Grover M, Edpao W, *et al*. Survival and morphology of auditory neurons in dissociated cultures of newborn mouse spiral ganglion. *Neuroscience.* 2006, 138: 653-662.

67. Alexander JK, Fuss B & Colello RJ. Electric field-induced astrocyte alignment directs neurite outgrowth. *Neuron & Glia Biology*. 2006, 2: 93-103.

68. Ayres CE, Jha BS, Meredith H, Bowman JR, Bowlin GL, Henderson SC, *et al*. Measuring fiber alignment in electrospun scaffolds: a user's guide to the 2D fast Fourier transform approach. Journal of biomaterials science. *Polymer edition*. 2008, 19: 603–621.

69. Taylor SA, Cao T, Talauliker PM & Lifshitz J. In Current Protocols Essential Laboratory Techniques. (eds S. R. Gallagher & E. A. Wiley) (Wiley, 2012).

70. Boström M, Khalifa S, Boström H, Liu W, Friberg U & Rask-Andersen H. Effects of neurotrophic factors on growth and glial cell alignment of cultured adult spiral ganglion cells. *Audiololgy & Neurootology*. 2010, 15: 175-86.

71. Rak K, Wasielewski N, Radeloff A, Scherzed A, Jablonka S, Hagen R, *et al*. Growth behavior of cochlear nucleus neuronal cells on semiconductor substrates. *J Biomed Mater Res A*. 2011, 97: 158-166.

72. Whitlon DS, Tieu D, Grover M, Reilly B & Coulson MT. Spontaneous association of glial cells with regrowing neurites in mixed cultures of dissociated spiral ganglia. *Neuroscience*. 2009, 161: 227-235.

73. Liu W, Boström M, Kinnefors A, Linthicum F & Rask-Andersen H. Expression of myelin basic protein in the human auditory nerve - an immunohistochemical and comparative study. *Auris Nasus Larynx*. 2012, 39 (1): 18-24.

74. Scwieger J, Esser KH, Lenarz T & Scheper V. Establishment of a long term spiral ganglion neuron culture with reduced glial cell number: Effects of AraC on cell composition and neurons. *Journal of Neuroscience Methods*. 2016, 268: 106-116.

75. Boström M, Anderson M, Lidholm D, Park KH, Schrott-Fischer A, Pfaller K, *et al*. Neural network and ganglion formations in vitro. *Otol. Neurotol*. 2007, 28: 1109-1119.

76. Jin Y, Kondo K, Ushio M, Kaga K, Ryan AF & Yamasoba T. Developmental changes in the responsiveness of rat spiral ganglion neurons to neurotrophic factors in dissociated culture: differential responses for survival, neuritogenesis and neuronal morphology. *Cell Tissue Research.* 2013, 351: 15–27.

77. Radotić V, Braeken D, Drviš P, Mattotti M, Kovačić D. Advantageous environment of micro-patterned, high-density complementary metal-oxide-semiconductor electrode array for spiral ganglion neurons cultured *in vitro*. *Sci Rep.* 2018, 8: 7446.

78. Anderson M, Boström M, Pfaller K, Glueckert R, Schrott-Fischer A, Gerdin B, *et al*. Structure and locomotion of adult in vitro regenerated spiral ganglion growth cones-A study using video microscopy and SEM. *Hearing research.* 2006, 215: 97-107.

79. Whitlon DS, Grover M, Tristano J, Williams T & Coulson MT. Culture conditions determine the prevalence of bipolar and monopolar neurons in cultures of dissociated spiral ganglion. *Neuroscience.* 2007, 146: 833-840.

80. Khalifa SAM, Björk P, Vieider C, Ulfendahl M & Scarfone E. Neuronal polarity mediated by micro-scale protein patterns and Schwann cells in vitro. *Tissue Engineering & Regenerative Medicine.* 2013, 10: 266–272.

81. Rask-Andersen H, Boström M, Gerdin B, Kinnefors A, Nyberg G, Engstrand T, *et al*. Regeneration of human auditory nerve. In vitro/in video demonstration of neural progenitor cells in adult human and guinea pig spiral ganglion. *Hearing research.* 2005, 203: 180-191.

82. Bruder JM, Lee AP & Hoffman-Kim D. Biomimetic materials replicating Schwann cell topography enhance neuronal adhesion and neurite alignment in vitro. *Journal of Biomater Sci Polym Ed.* 2007, 18: 967-982.

83. Dowell-Mesfin NM, Abdul-Karim MA, Turner AMP, Schanz S, Craighead HG, Roysam B, *et al*. Topographically modified surfaces affect orientation and growth of hippocampal neurons. *Journal of Neural Engineering.* 2004, 1: 78–90.

84. Romand R & Romand MR. Qualitative and quantitative observations of spiral ganglion development in the rat. *Hearing Research.* 1985, 1: 111-20.

85. Mo ZI & Davis RL. Endogenous firing patterns of murine spiral ganglion neurons. *J Neurophysiol.* 1997, 77: 1294-305.

86. Liu Q & Davis RL. Regional specifications of threshold sensitivity and response time in CBA/CaJ mouse spiral ganglion neurons. *J Neurophysiol.* 2007, 98: 2215-2222.

87. Markowitz AL & Kalluri R. Gradients in the biophysical properties of neonatal auditory neurons align with synaptic contact position and the intensity coding map of inner hair cells. *eLife.* 2020, 9: e55378.

88. Zhou Z, Liu Q & Davis RL. Complex regulation of spiral ganglion neuron firing patterns by neurotrophin-3. *J Neurosci: Official J Soc Neurosci.* 2005, 25: 7558-66.

89. Needham K, Nayagam BA, Minter RL, & O'Leary SJ. Combined application of brain-derived neurotrophic factor and neurotrophin-3 and its impact on spiral ganglion neuron firing properties and hyperpolarization-activated currents. *Hearing Research.* 2012, 291: 1-14.

90. Lewandowska MK, Bakkum DJ, Rompani SG & Hierlemann A. Recording large extracellular spikes in microchannels along many axonal sites from individual neurons. *PLoS One.* 2015, 10: e0118514.

91. Markowitz AL, Iyer MG & Kalluri R. Patch-clamp recordings and single fiber labeling from spiral ganglion somata in acutely prepared semi-intact cochleae from neonatal rats. *Bio-protocol.* 2022, 12: e4281.

92. Adamson CL, Reid MA, Mo ZL, Bowne-English J & Davis RL. Firing features and potassium channel content of murine spiral ganglion neurons vary with cochlear location. *J Comp Neurol.* 2002b, 447: 331-350.

93. Hahnewald S, Roccio M, Tscherter A, Streit J, Ambett R & Senn P. Spiral ganglion neuron explant culture and electrophsiology on multi electrode arrays. *J Vis Exp.* 2016, 116: e54538.

94. Miccoli B, Lopez CM, Goikoetxea E, Putzeys J, Sekeri M, Krylychkina O, *et al*. High-density electrical recording and impedance imaging with a multi-modal CMOS multi-electrode array chip. *Front. Neurosci.* 2019, 13: 641.

8. ABSTRACT

Objectives:

This study investigated a micro-patterned, high-density complementary metal–oxide semiconductor (CMOS) electrode array to be used as a biologically permissive environment for organization, guidance, and simultaneous electrical stimulation and recording of spiral ganglion neurons (SGN).

Methods:

SGNs extracted and isolated from cochleae of P5-P7 rat pups and adult guinea pigs were cultured for 1, 4, and 7 days *in vitro* on glass coverslips (control) and CMOS electrode array. The cultures were analyzed visually and immunohistochemically for SGN presence, outgrowth, neurite alignment, neurite length, neurite asymmetry, and the contact of neuronal soma and neurites with the microelectrodes. Electrophysiological experiments were performed at 37° using a CMOS-like electrode array in two modes. The first, spontaneous, mode focuses on recording intrinsic spontaneous electrophysiological activity without external stimulation to determine whether cells can fire action potentials in the absence of a standard neurotransmitting mechanism via hair cells, while the second, stimulation mode recorded potential cell responses to an electrical biphasic stimulus (positive phase first) with a total duration of 60 μs and an amplitude of 500 nA or 800 nA.

Results:

Our findings indicate that the topographical environment of the CMOS chip with micro-patterned pillars enhanced growth, survival, morphology, neural orientation, and alignment of SGNs *in vitro* compared to control. Smaller spacing (0.8-1.6 μm) between protruding pillars on CMOS led SGNs to develop structured and guided neurites oriented along three topographical axes separated by 60°. These results constitute a morphological basis for positioning the microelectrodes on the chip appropriate for direct contact with SGNs. This configuration allowed the CMOS electrode array to electrically stimulate the SGN, whose responses were observed with live Fluo 4 calcium imaging and, at the same time, recorded electrophysiologically using the same CMOS electrode array. The average maximum spike amplitude was 135.4 ± 15.2 μV for recorded spontaneous activity and 130 ± 10 μV for recorded neural activity after stimulation.

Conclusion:

To the best of our knowledge, this study demonstrates for the first time that simultaneous stimulation and recording with the same electrode array is feasible for measuring auditory neuronal activity from dissociated SGNs. Immunostaining of SGNs cultures grown on a CMOS electrode array for the neuronal marker Tuj revealed both somata and processes of neurons on the electrode surface, in

66

accordance with results that the position of neuronal soma and neurites affects recordings of electrical activity on the CMOS electrode array. The model presented in this study represents a novel *in vitro* tool to investigate strategies for simultaneous electrical stimulation and recording of auditory neurons to optimize CI technology.

9. SAŽETAK

Naslov: Morfološka i elektrofiziološka karakterizacija stanica spiralnog ganglija *in vitro* uzgojenih na komplementarnom poluvodiču sa elektrodnim sustavima visoke gustoće.

Cilj:

Ova studija istraživala je mogućnost korištenja elektrodnog sustava visoke gustoće temeljenog na CMOS tehnologiji, kao biološki prihvatljivog okruženja za organizaciju, navođenje te električnu stimulaciju živčanih stanica spiralnog ganlija (*engl*. SGNs).

Metode:

Stanice spiralnog ganglija, ekstrahirane i izolirane iz pužnica 5-7 dana starih (P5-P7) štakorskih mladunaca i odraslih zamoraca, uzgajane su 1, 4 i 7 dana *in vitro* na stakalcima (kontrola) te CMOS čipovima. Kulture su analizirane vizualno i imunohistokemijski na prisutnost živčanih stanica spiralnog ganglija, na rast, poravnanje neurita, duljinu neurita, asimetriju neurita te kontakt neuronske some i neurita sa elektrodama. Elektrofiziološki pokusi izvedeni su na 37°C u dva eksperimentalna modusa sa svrhom detekcije živčane aktivnosti koristeći elektrodni sustav koji se temelji na CMOS-u. Prvi modus je usredotočen na snimanje intrizične, spontane elektrofiziološke aktivnosti bez vanjske stimulacije kako bi se utvrdilo mogu li neuroni generirati akcijske potencijale u odsutnosti standardnog mehanizma neurotransmisije putem osjetilnih slušnih stanica. Drugi modus je uključivao stimulaciju pomoću koje su bili zabilježeni potencijalni stanični odgovori na električni bifazični podražaj (s prvom pozitivnom fazom) s ukupnim trajanjem od 60 µs i amplitudom od 500 nA ili 800 nA.

Rezultati:

Rezultati pokazuju, da je topografsko okruženje CMOS čipa sa mikroiglicama poboljšalo rast, preživljavanje, morfologiju te neuralnu orientaciju *in vitro* uzgojenih živčanih stanica spiralnog ganglija u usporedbi sa kontrolom. Manji razmak (0.8-1.6 µm) između mikroiglica na CMOS čipu doveo je stanice spiralnog ganglija do razvoja strukturiranih i vođenih neurita usmjerenih duž tri topografske osi pomaknutih za 60°. Ti rezultati čine morfološku osnovu za pozicioniranje mikroelektroda na čipu prikladnih za izravan kontakt sa stanicama spiralnog ganglija. Ova konfiguracija je omogućila uspješnu električnu stimulaciju stanica spiralnog ganglija čiji su odgovori promatrani uživo pomoću Fluo 4 oslikavanja kalcija na CMOS čipu. Prosječna maksimalna vršna amplituda je bila 135.4 ± 15.2 µV za zabilježenu spontanu aktivnost te 130 ± 10 µV za zabilježenu živčanu aktivnost nastalu kao odgovor na stimulaciju.

Zaključak:

Ova studija pokazuje da je istovremena stimulacija te snimanje s istim elektrodnim sustavom elektroda visoke gustoće izvedivo za mjerenje elektrofiziološke aktivnosti živčanih stanica dobivenih iz *in vitro* kultura stanica spiralnog ganglija. Imunohistokemijsko bojanje kultura uzgojenih na CMOS čipu za neuronski marker Tuj otkrilo je tijela stanica (some) i procese (neurite) neurona na površini elektroda, te u skladu s rezultatima, pokazuje, da položaj neurona i neurita utječe na snimanje električne aktivnosti na CMOS čipu. Model predstavljen u ovoj studiji predstavlja pogodan *in vitro* alat za istraživanje stimulacijskih protokola za istovremenu električnu stimulaciju i snimanje živčanih stanica spiralnog ganglija u svrhu optimizacije tehnologije kohlearnih implantata (*engl*. CI).

10. CURRICULUM VITAE

PERSONAL INFORMATION

Name and surname: Viktorija Radotić

E-mail: viktorija.radotic@gmail.com

Citizenship: Slovene

Place and date of birth: 12th of January, Postojna, Slovenia

EDUCATION

2016-today   Doctoral study (PhD) Translational Research in Biomedicine, University of Split, School of Medicine, Split

2011-2014   Master study Structural and Functional Biology, University of Ljubljana, Biotechnical faculty, Ljubljana

2008-2011   Graduate study Biology, University of Ljubljana, Biotechnical faculty, Ljubljana

WORK EXPERIENCE

January 2018-December 2018   Assistant at University of Split, Center of Excellence for Science and Technology-Integration of Mediterranean region (STIM-REI project), development of new graphene materials for micro-electronic chips

September 2017-December 2017   Researcher at University of Split, Faculty of Science, Split, PhD student, research in the field of hearing

December 2016-May 2017   Researcher at IRI center d.o.o. (Entrepreneurship and Innovation), Split, PhD student, scientific research, preparation of project documentation, coordination and administration of the projects

October 2015-November 2016   Scientific researcher, PhD student at University of Split, School of Medicine, Split, research in the field of hearing (project EvoNa), *in vitro* cultures of primary auditory neurons, neurophysiological research of auditory neurons using micro-electronic chips

MOTHER LANGUAGE

- Slovene

OTHER LANGUAGES

- Croatian

- English

- German

- Spanish

PROFESSIONAL DEVELOPMENT/TRAINING

- 2019: imec, Leuven, Belgium: professional training for cell physiology (microelectrode array)

- 2019: 56th Inner Ear Biology Workshop (Padua, Italy), poster presentation with title: Stimulation of spiral ganglion neurons cultured *in vitro* with a global electro-magnetic field

- 2018: Conference for public of the STIM-REI project (Quarterly gathering of young researches, University of Split, Faculty of Science), participant

- 2018: 55th Inner Ear Biology Workshop (Berlin, Germany), poster presentation with title: Characterization of spiral ganglion neurons cultured on 3D complementary metal-oxide-semiconductor chips

- 2017: Congress „Advances in Biomedical Research (Medils, Split, Croatia), poster presentation with title: Characterization of spiral ganglion neurons cultured on 3D complementary metal-oxide-semiconductor chips

- 2017: Course Project cycle management, Split, Croatia

- 2017: Course Entrepreneurship competencies for innovative endeavours, Split, Croatia

- 2016: Laboratory animal science course, Split, Croatia: license for work with experimental animals (FELASA, cat. C equivalent)

- 2016: Carl-Ludwig Institute for Physiology, Leipzig, Germany: professional training for cell physiology (patch-clamp)

- 2016: Summer school „Medical Bionics for Hearing (Split, Croatia), oral presentation with title: Morphological characterization of spiral ganglion neurons cultured on CMOS chips and silicon micro-pillar substrates

- 2016: Congress „14th European Balkan Congress" (Hearing Implants & High Tech Hearing Aids, Split, Croatia), participant

- 2016: Symposium „Molecular life of stem cells" (Helmholtz Zentrum Műnchen, Ljubljana, Slovenia), participant

- 2015: Symposium „Suvremeni pristup dijagnostici i liječenju oštečenja sluha (KBC Split, Croatia), participant

- 2014: Symposium „Stem cell plasticity" (Helmholtz Zentrum Műnchen, Ljubljana, Slovenia), participant

- 2013: Syposium „Superresolution Microscopy" (CIPkePiB, Ljubljana, Slovenia); participant